

Remarks on the Stress Version of Topology Optimization of Truss Structures

Sławomir CZARNECKI

*Department of Structural Mechanics and Computer Aided Engineering,
Faculty of Civil Engineering, Warsaw University of Technology, Warsaw, Poland,
e-mail: slawomir.czarncki@pw.edu.pl*

Based on numerical solutions that minimize the total potential energy of trusses subjected to static loads, with specified displacements at selected support nodes and simultaneous fulfillment of the isoperimetric condition on the structure's volume, several properties of optimally designed structures are revealed. The most significant finding is the relatively frequent occurrence of non-unique global solutions, represented as vectors of cross-sectional areas of members in the stress-based version of topology optimization problem. A key aspect of the presented method is the objective function, derived from Castigliano's theorem, which minimizes the total potential energy. Unlike traditional approaches that optimize transverse areas of the members, this method uses statically admissible forces in the truss members as design variables. This formulation allows for a free search of solutions, including cases where certain members can disappear in the optimal design. Numerous tests have revealed an interesting property of the objective function, indicating that global solutions are located at the bottom of a long valley in its graph within the space R^{r+1} , where r denotes the size of the kernel of the equilibrium matrix governing the force balance equations of the nodes of the truss structure.

Keywords: topology optimization, trusses, prescribed displacements, non-uniqueness of optimal solutions, narrow valley.



Copyright © 2025 The Author(s).
Published by IPPT PAN. This work is licensed under the Creative Commons Attribution License
CC BY 4.0 (<https://creativecommons.org/licenses/by/4.0/>).

1. Introduction

The problem of designing the stiffest structures, assuming an upper bound on the available material (or equivalently, bounding the manufacturing cost of such structures), has been one of the most extensively explored areas of scientific research in the field of structure optimization for several decades. In particular, a significant body of work has been devoted to determining the optimal cross-sectional areas of members and/or the optimal locations of truss structure nodes under a given nodal load. See, e.g., papers [1–13] among the hundreds,

if not more, of scientific articles addressing the optimal design of truss structures since the beginning of the 20th century. However, most of the optimal design problems concern cases where trusses are subjected to static loads alone, while ignoring potential kinematic loads at selected support nodes. In general, it is commonly assumed that the positions of internal (free) nodes are fixed, while the positions of support nodes can be adjusted by imposing given displacements (e.g., due to support settlements). In these cases, the non-negative stiffnesses of the members (i.e., assuming that they can also reach zero values) are treated as design variables, while the total volume of the truss represents the design cost. The assumption that stiffnesses are non-negative leads to the classical problem of topology optimization for engineering structures.

In the paper [14], an original algorithm based solely on member forces was presented for searching the optimal cross-sectional areas of truss members subjected to both static and kinematic loads. This was done under the constraint on the sum of the stiffness of its members, equivalent to the constraint on the volume of the truss (i.e., its cost), assuming the Young modulus of the material from which all members are made is fixed and uniform across all members. In [14], it was also point out that, until 2010, almost no articles on the topological optimization of trusses discussed the cases involving kinematic loads or simultaneous kinematic-static loads. Correct methods for optimizing elastic bodies (in particular, truss structures) in the presence of kinematic loads were only proposed in [15–18] after 2010. The correctness of the posed problem, especially in the context of the stress approach used in this paper, stems primarily from the fact that minimizing over all statically admissible forces in the truss members – parameters of Castigliano’s total potential energy – leads to a minimizer (optimal vector of forces in the truss members). This minimizer is a solution to the statics problem of a truss subjected to both static and kinematic loads. Additionally, and importantly, this functional can (and should) be a starting point for formulating the truss topology optimization problem, because the objective function derived from it and the solutions obtained through its minimization have clear, explicit, logical and, above all, consistent properties from a physical interpretation standpoint (this will be very briefly explained later in the text). The method proposed in [14] reduces the problem of topology optimization of truss structures to finding the minimum of a certain functional without any additional constraint conditions, whose only design variable (in the presence of both static and/or kinematic loads) is the vector of statically admissible member forces. More precisely, the design variable is an r -dimensional vector of real numbers, whose components when multiplied by the basis vectors spanning the kernel of the truss equilibrium matrix (of kernel dimension r) together with some arbitrary particular solution of the equilibrium equation, ultimately determine the statically admissible set of forces in the truss members. Once the minimizer of

this functional is found, the optimal values of the truss cross-sectional areas for both static and kinematic loads are computed based on the derived analytical formulas. An important feature of the method proposed in [14] is that, without imposing additional corrective conditions, which would be necessary if the design parameters explicitly depended on the components of the displacement vector, the members are allowed to disappear in the final optimal solution. However, in the present author's opinion, the trade-off for not having to redefine the topology of node connections with rods due to the disappearance of some members during subsequent iterations is the challenge of precisely locating the minimizers of the convex objective function. These issues arise during numerical tests, particularly when only static loads, only kinematic loads, or both are present.

The main goal of this work is to clarify the emergence of these problems by using the results of numerous numerical tests for problems where the dimension of the equilibrium matrix kernel is exactly 2 (which does not imply an equally small number of rods in the truss, as there can be any number of rods in principle).

The final (additional but highly relevant) example shows the numerical results of topology optimization for an L-shaped cantilever, subjected only to static loads and made of a non-homogeneous, isotropic, linear-elastic material. These results are obtained using the isotropic material design (IMD) method, which is analogous to the one used for trusses to search for the distribution of elastic modulus fields. The IMD method is a stress-based version of topology optimization for non-homogeneous, isotropic elastic bodies under the isoperimetric condition, as presented in [19]. This example is important because the analysis of the obtained results clearly indicates a very similar nature of the objective function to that of truss structures, and highlights the resulting difficulties in numerical analysis.

The paper also points out other interesting features of optimal solutions, especially within the geometric-linear theory of trusses (and thus the geometric-linear theory of elastic bodies) loaded kinematically or kinematically and statically. This suggests the need to stop the practice of treating the equilibrium equations in the undeformed configuration as sufficiently justified and correct relations in the context of topology optimization.

2. Optimum design of planar and spatial trusses

Before presenting examples of optimal topologies of lattice structures, the basic formulas defining the method of minimizing total potential energy will be briefly derived, with only slight changes in notation compared to that in [14].

According to Fig. 1, we introduce the following notation for forces, displacements and other parameters required to describe the statics of truss structures

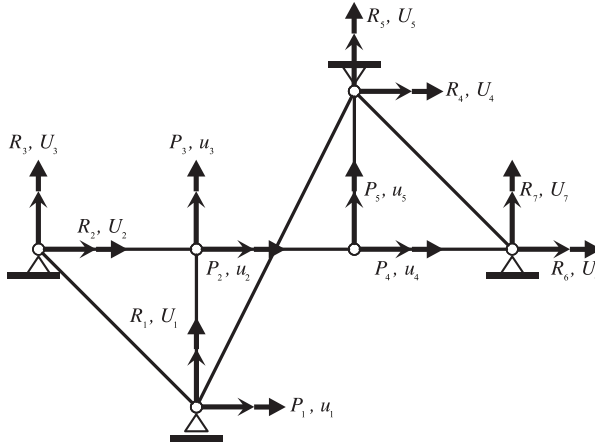


FIG. 1. Illustrative eight-member truss structure ($e = 8$), with seven support reactions ($m = 7$), and five unknown displacements ($s = 5$) (three non-sliding pin supports, one pin support with possible horizontal displacement, and two free nodes).

with e members, m prescribed displacements U_1, \dots, U_m , and unknown support reactions R_1, \dots, R_m , as well as s unknown displacements u_1, \dots, u_s and given loads P_1, \dots, P_s . Let $\mathbf{U} = (U_1, \dots, U_m)$ and $\mathbf{R} = (R_1, \dots, R_m)$ be the vectors of known displacements at supports and unknown support reactions, respectively, $\mathbf{u} = (u_1, \dots, u_s)$ and $\mathbf{P} = (P_1, \dots, P_s)$ be the vectors of unknown nodal displacements and given loads, respectively, $\mathbf{N} = (N_1, \dots, N_e)$ and $\mathbf{\Delta} = (\Delta_1, \dots, \Delta_e)$ be the vectors of unknown member forces and elongations of members, respectively, $\mathbf{x} = (x_1, \dots, x_e)$, $x_k = EA_k l_k \geq 0$, $k = 1, \dots, e$, be the vector of design parameters, where $E > 0$ represents Young's modulus, $A_k \geq 0$, $l_k > 0$ denote the cross-sectional area and length of the k -th member, respectively.

The nodes are a priori given, i.e., their positions are fixed. Therefore, the distances l_k between nodes are not parameters of the task and can only be interpreted as constant multipliers. By defining the design variable x_k as $EA_k l_k$ instead of EA_k , we can state that the k -th member may not exist when $x_k = 0$, rather than assuming that the k -th member exists but has zero stiffness, which seems to be consistent with the physical interpretation of the main feature of the presented optimization algorithm, which allows, without practically any additional mathematical constraints, the possibility of removing members during the optimization process. This, in turn, allows for a change in the initial topology of connections between nodes in the optimal solution. Allowing some members to disappear is a crucial assumption. We adopt the standard notation for geometric matrices: $\bar{\mathbf{B}} = (\bar{B}_{ij})_{e \times s}$, $\bar{\bar{\mathbf{B}}} = (\bar{\bar{B}}_{ij})_{e \times m}$ involving directional cosines, and for diagonal matrix: $\mathbf{E} = (E_{ij})_{e \times e} = \text{diag} \left\{ \frac{EA_k}{l_k} \right\}_{k=1, \dots, e}$.

Equilibrium equations:

$$\bar{\mathbf{B}}^T \mathbf{N} = \mathbf{P}, \quad \bar{\bar{\mathbf{B}}}^T \mathbf{N} = \mathbf{R}, \quad (1)$$

together with constitutive and geometric relationships:

$$\mathbf{N} = \mathbf{E}\boldsymbol{\Delta}, \quad \boldsymbol{\Delta} = \bar{\mathbf{B}}\mathbf{u} + \bar{\bar{\mathbf{B}}}\mathbf{U} \quad (2)$$

formulate the statics problem for geometrically linear truss structures.

We will assume that the vector of design parameters $\mathbf{x} \in R^e$ satisfies the following isoperimetric condition:

$$\mathbf{x} \in \Xi, \quad (3)$$

where for any given number $\Lambda > 0$,

$$\Xi = \left\{ \mathbf{x} = (x_1, \dots, x_e) : \forall k, x_k \geq 0 \wedge \sum_{k=1}^e x_k \leq \Lambda \right\} \quad (4)$$

is the set of the admissible design parameters.

The above equations can be aggregated to a single equation:

$$\hat{\mathbf{K}}\hat{\mathbf{u}} = \hat{\mathbf{P}}, \quad (5)$$

where the matrix is defined as:

$$\hat{\mathbf{K}} = (\hat{K}_{ij})_{(s+m) \times (s+m)} = \begin{bmatrix} \bar{\mathbf{B}}^T \mathbf{E} \bar{\mathbf{B}} & \bar{\mathbf{B}}^T \mathbf{E} \bar{\bar{\mathbf{B}}} \\ \bar{\bar{\mathbf{B}}}^T \mathbf{E} \bar{\mathbf{B}} & \bar{\bar{\mathbf{B}}}^T \mathbf{E} \bar{\bar{\mathbf{B}}} \end{bmatrix} \quad (6)$$

and

$$\hat{\mathbf{u}} = \left(\underbrace{\hat{u}_1, \dots, \hat{u}_s}_{\mathbf{u}}, \underbrace{\hat{u}_{s+1}, \dots, \hat{u}_{s+m}}_{\mathbf{U}} \right) = (\mathbf{u}, \mathbf{U}), \quad (7)$$

$$\hat{\mathbf{P}} = \left(\underbrace{\hat{P}_1, \dots, \hat{P}_s}_{\mathbf{P}}, \underbrace{\hat{P}_{s+1}, \dots, \hat{P}_{s+m}}_{\mathbf{R}} \right) = (\mathbf{P}, \mathbf{R}).$$

It is obvious that in the above formulation:

$$\mathbf{u} = \mathbf{u}(\mathbf{x}), \quad \mathbf{R} = \mathbf{R}(\mathbf{x}), \quad (8)$$

because $\mathbf{E} = \mathbf{E}(\mathbf{x})$, and thus $\hat{\mathbf{K}} = \hat{\mathbf{K}}(\mathbf{x})$.

Let, for any but fixed $\mathbf{x} \in \Xi$,

$$\begin{aligned} \hat{\mathbf{u}}^* &= \hat{\mathbf{u}}^*(\mathbf{x}) = \begin{bmatrix} \mathbf{u}^*(\mathbf{x}) \\ \mathbf{U} \end{bmatrix} \in R^{s+m} \quad \text{and} \\ (\mathbf{u}^*, \Delta^*, \mathbf{N}^*, \mathbf{R}^*) &= (\mathbf{u}^*, \Delta^*, \mathbf{N}^*, \mathbf{R}^*)(\mathbf{x}) \end{aligned} \quad (9)$$

be the solution:

$$\widehat{\mathbf{K}}(\mathbf{x})\hat{\mathbf{u}}^*(\mathbf{x}) = \widehat{\mathbf{P}} \quad (10)$$

to problem (1), i.e.,

$$\begin{aligned} \mathbf{u}^*(\mathbf{x}) &= \mathbf{K}^{-1}(\mathbf{x})\mathbf{P}, \quad \mathbf{K}(\mathbf{x}) = \overline{\mathbf{B}}^T \mathbf{E}(\mathbf{x})\overline{\mathbf{B}}, \\ \Delta^*(\mathbf{x}) &= \overline{\mathbf{B}} \mathbf{u}^*(\mathbf{x}) + \overline{\mathbf{B}} \mathbf{U}, \quad \mathbf{N}^*(\mathbf{x}) = \mathbf{E}\Delta^*(\mathbf{x}), \quad \mathbf{R}^*(\mathbf{x}) = \overline{\overline{\mathbf{B}}}^T \mathbf{N}^*(\mathbf{x}). \end{aligned} \quad (11)$$

We consider the topology optimization problem as follows: for known vectors

$$\mathbf{P} \in R^s, \quad \mathbf{U} \in R^m, \quad (12)$$

find the vector

$$\mathbf{x} = (x_1, \dots, x_e) \in \Xi, \quad (13)$$

i.e., equivalently find all cross-sectional areas

$$A_k = \frac{x_k}{El_k} \geq 0, \quad k = 1, \dots, e, \quad (14)$$

minimizing the total potential energy

$$\varphi : \Xi \rightarrow \mathbb{R}, \quad \forall \mathbf{y} \in \Xi, \quad \varphi(\mathbf{y}) = \underbrace{\mathbf{P} \cdot \mathbf{u}^*(\mathbf{y})}_{\text{compliance}} - \mathbf{R}^*(\mathbf{y}) \cdot \mathbf{U}, \quad (15)$$

as described in [17]. The assumption that Young's modulus $E > 0$ is constant, reduces the above problem to the minimization of the total potential energy, assuming that the volume of all truss members does not exceed the allowable value

$$\sum_{k=1}^e A_k l_k \leq \frac{\Lambda}{E}. \quad (16)$$

In other words, we are looking for the solution $\mathbf{x}^* \in \Xi$ to the following problem:

$$\varphi^* = \min_{\mathbf{x} \in \Xi} (\mathbf{P} \cdot \mathbf{u}^*(\mathbf{x}) - \mathbf{R}^*(\mathbf{x}) \cdot \mathbf{U}), \quad \mathbf{x}^* = \arg \min_{\mathbf{x} \in \Xi} \varphi(\mathbf{x}) \in \Xi. \quad (17)$$

How can we most convincingly justify the choice of the objective function in the presented problem to make it physically plausible? The simplest justification is as follows. Firstly, in the case when all possible displacements \mathbf{U} of the supports are equal to zero, the minimization:

$$\min_{\mathbf{x} \in \Xi} \varphi(\mathbf{x}) = \min_{\mathbf{x} \in \Xi} \mathbf{P} \cdot \mathbf{u}^*(\mathbf{x}) \quad (18)$$

guarantees that the designed truss will be stiff, because the work of known forces \mathbf{P} on the displacements of nodes $\mathbf{u}^*(\mathbf{x})$ caused by them is minimized. This is interpreted as the compliance minimization. Secondly, in the case when only known displacements \mathbf{U} are applied to selected nodes of the supports, the work of nodal reactions on the known displacements of these nodes is maximized:

$$\min_{\mathbf{x} \in \Xi} \varphi(\mathbf{x}) = \min_{\mathbf{x} \in \Xi} (-\mathbf{R}^*(\mathbf{x}) \cdot \mathbf{U}) = -\max_{\mathbf{x} \in \Xi} (\mathbf{R}^*(\mathbf{x}) \cdot \mathbf{U}), \quad (19)$$

which can be interpreted as the maximization of reaction forces $\mathbf{R}^*(\mathbf{x})$ that provide the greatest resistance to the known displacements \mathbf{U} . The third justification requires recalling the Castigliano functional and its role in the alternative, final formulation of the statics problem for geometrically linear elastic bodies.

So, let us introduce the Castigliano functional:

$$\begin{aligned} \mathcal{J} : \Theta_+ \times \Sigma &\rightarrow R, \quad \forall (\mathbf{x}, \mathbf{N}) \in \Theta_+ \times \Sigma, \\ \mathcal{J}(\mathbf{x}, \mathbf{N}) &= \frac{1}{2} \mathbf{N} \cdot (\mathbf{E}^{-1}(\mathbf{x}) \mathbf{N}) - \left(\overline{\mathbf{B}}^T \mathbf{N} \right) \cdot \mathbf{U} \end{aligned} \quad (20)$$

for the truss structure loaded both statically and kinematically, where:

$$\Sigma = \left\{ \mathbf{N} \in R^e : \overline{\mathbf{B}}^T \mathbf{N} = \mathbf{P} \right\} \quad (21)$$

is the set of all statically admissible member forces, and

$$\Theta_+ = \left\{ \mathbf{x} = (x_k) \in R^e : \forall k, x_k = EA_k l_k > 0 \right\} \quad (22)$$

is the set of all positive parameters defining the all positive cross-sections A_k , wherein

$$\Xi \not\subset \Theta_+, \quad \Xi \cap \Theta_+ \neq \emptyset. \quad (23)$$

Then, the search for a solution to the problem:

$$\varphi^* = \min_{\mathbf{x} \in \Xi} \varphi(\mathbf{x}) \quad (24)$$

can be carried out in a different way, using Castigliano's theorem, i.e.,

$$\varphi^* = \min_{\mathbf{x} \in \Xi} \varphi(\mathbf{x}) = 2 \min_{\mathbf{x} \in \Xi} \min_{\mathbf{N} \in \Sigma} \mathfrak{J}(\mathbf{x}, \mathbf{N}). \quad (25)$$

Based on this fundamental relationship, it can be shown that after changing the order of minimization from $\min_{\mathbf{x} \in \Xi} \min_{\mathbf{N} \in \Sigma}(\dots)$ to $\min_{\mathbf{N} \in \Sigma} \min_{\mathbf{x} \in \Xi}(\dots)$ in the above double minimization, the problem reduces to:

$$\varphi^* = \min_{\mathbf{N} \in \Sigma} F(\mathbf{N}), \quad \mathbf{N}^* = \arg \min_{\mathbf{N} \in \Sigma} F(\mathbf{N}) \in \Sigma, \quad (26)$$

where

$$\begin{aligned} F: \Sigma &\rightarrow \mathbb{R} \quad \forall \mathbf{N} = (N_1, \dots, N_e) \in \Sigma, \\ F(\mathbf{N}) &= \min_{\mathbf{x} \in \Xi} \left\{ \mathbf{N} \cdot \mathbf{E}^{-1}(\mathbf{x})\mathbf{N} - 2 \left(\overline{\overline{\mathbf{B}}}^T \mathbf{N} \right) \cdot \mathbf{U} \right\} \\ &= \frac{\left(\sum_{k=1}^e |N_k| l_k \right)^2}{\Lambda} - 2 \left(\overline{\overline{\mathbf{B}}}^T \mathbf{N} \right) \cdot \mathbf{U}, \\ \arg \min_{\mathbf{x} \in \Xi} \left\{ \mathbf{N} \cdot \mathbf{E}^{-1}(\mathbf{x})\mathbf{N} - 2 \left(\overline{\overline{\mathbf{B}}}^T \mathbf{N} \right) \cdot \mathbf{U} \right\} &= \mathbf{x}^{\mathbf{N}} = (x_k^{\mathbf{N}}), \\ x_k^{\mathbf{N}} &= \frac{\Lambda |N_k| l_k}{\sum_{i=1}^e |N_i| l_i}, \end{aligned} \quad (27)$$

is the new objective function, not involving any design variables. This new problem has been obtained by a strict mathematical procedure. Its physical meaning, however, remains unclear. This procedure can be found in the book [2] in the case of compliance minimization, see also [5, ch. 2]. The present paper, along with the paper [14], extends the same idea to the problem of minimizing the total potential energy corresponding to loads other than nodal forces. A more detailed mathematical derivation of relationship (27) can be found, among others, in [14, sec. 4.2, p. 6].

Once the minimizer

$$\mathbf{N}^* = (N_1^*, \dots, N_e^*) \in \Sigma \quad (28)$$

of F is found, then

$$\mathbf{x}^* = \mathbf{x}^{\mathbf{N}^*}, \quad (29)$$

i.e.,

$$\left. \begin{aligned} x_k^* &= \frac{\Lambda |N_k^*| l_k}{\sum_{i=1}^e |N_i^*| l_i} \\ x_k^* &= EA_k^* l_k \end{aligned} \right\} \Rightarrow A_k^* = \frac{\Lambda}{E} \frac{|N_k^*|}{\sum_{i=1}^e |N_i^*| l_i}, \quad k = 1, \dots, e, \quad (30)$$

is the solution to the topology optimization problem. We conclude that the absolute value of the optimal stress in each k -th member is constant, i.e.,

$$|\sigma_k^*| = \frac{|N_k^*|}{A_k^*} = \frac{E \sum_{i=1}^e |N_i^*| l_i}{\Lambda} = \text{const.} \quad (31)$$

For the given truss structure and known loading \mathbf{P} , any statically admissible member force \mathbf{N} can be associated with a vector:

$$\boldsymbol{\alpha} = (\alpha_1, \dots, \alpha_r) \in R^r. \quad (32)$$

Indeed, if

$$\bar{\mathbf{N}} = (\bar{N}_1, \dots, \bar{N}_e) \in R^e \quad (33)$$

is any particular solution of the equilibrium equation:

$$\bar{\mathbf{B}}^T \mathbf{N} = \mathbf{P} \quad (34)$$

and the vectors

$$\mathbf{h}_k = (h_{k_1}, \dots, h_{k_e}) \in R^e \quad (35)$$

($k = 1, \dots, r$) span the kernel of the equilibrium matrix $\bar{\mathbf{B}}^T$ (generally a rectangular matrix with the number of rows less than the number of columns), then any statically admissible $\mathbf{N} \in \Sigma$ can be represented as:

$$\mathbf{N} = \bar{\mathbf{N}} + \sum_{k=1}^r \alpha_k \mathbf{h}_k, \quad (36)$$

where $r = \dim \ker \bar{\mathbf{B}}^T$. All vectors \mathbf{N} , $\bar{\mathbf{N}}$, and \mathbf{h}_k whose components satisfy the equilibrium equation (34), define, of course, all statically admissible member forces.

In other words, any statically admissible solution \mathbf{N} can be identified with a certain vector $\boldsymbol{\alpha}$, and therefore, the minimization of functional $F(\mathbf{N})$ over statically admissible member forces $\mathbf{N} \in \Sigma$ can be reduced to its minimization over all vectors $\boldsymbol{\alpha}$. This leads to a fully unconstrained minimization problem, for which known and effective numerical methods can be applied.

Therefore, the minimized functional F will be formally replaced with an equivalently defined functional J as follows:

$$J: R^r \rightarrow R,$$

$$\forall \boldsymbol{\alpha} = (\alpha_1, \alpha_2, \dots, \alpha_r) \in R^r, \quad J(\boldsymbol{\alpha}) = \frac{\left(\sum_{k=1}^e |N_k(\boldsymbol{\alpha})| l_k \right)^2}{2\Lambda} - \left(\bar{\mathbf{B}}^T \mathbf{N}(\boldsymbol{\alpha}) \right) \cdot \mathbf{U}, \quad (37)$$

where

$$\mathbf{N}(\boldsymbol{\alpha}) = (N_1(\boldsymbol{\alpha}), \dots, N_e(\boldsymbol{\alpha})) \in R^e, \quad N_k(\boldsymbol{\alpha}) = \bar{N}_k + \sum_{i=1}^r \alpha_i h_{ik}, \quad k = 1, \dots, e. \quad (38)$$

Then,

$$F^* = 2J^*, \quad (39)$$

where

$$J^* = \min_{\boldsymbol{\alpha} \in R^r} J(\boldsymbol{\alpha}), \quad \boldsymbol{\alpha}^* = (\alpha_i^*) = \arg \min J(\boldsymbol{\alpha}) \quad (40)$$

and finally

$$\mathbf{N}^*(\boldsymbol{\alpha}) = (N_1(\boldsymbol{\alpha}^*), \dots, N_e(\boldsymbol{\alpha}^*)) = \left(\bar{N}_k + \sum_{i=1}^r \alpha_i^* h_{ik} \right). \quad (41)$$

3. Optimum design of two-dimensional, non-homogeneous, isotropic elastic bodies

The presentation of the distributions of cross-sectional areas $A_k^* \geq 0$, $k = 1, \dots, e$, of members in several selected examples of truss structures will be preceded by a very brief description of the analogous problem in stress-based topology optimization of linearly elastic, non-homogeneous, isotropic elastic bodies. This will help to reveal, in the last example, similar numerical problems in truss structures when searching for the global minimum of the compliance function. These problems probably result from the fact that, after interpolating statically admissible stresses (analogous to the interpolation of kinematically admissible displacements in the classical version of FEM), the ‘graph’ of the minimized functional very often has a ‘shape’ resembling a long flat valley in the s -dimensional ($s \gg 2$) kernel space of the rectangular matrix defining the equilibrium of a 2D or 3D body.

Assuming that only a static load \mathbf{t} is applied to the continuum body Ω on a fragment of its boundary Γ_1 (for simplicity, we assume that kinematic loads are absent), the analogue of the truss topology optimization becomes the problem of searching for the optimal distribution of the bulk $k(x) \geq 0$ and shear $\mu(x) \geq 0$ moduli, which are involved in the representation of the non-homogeneous isotropic fourth-rank Hooke’s tensor $\mathbf{C} = \mathbf{C}(x)$, $x \in \Omega$ and minimizing the compliance:

$$f(\mathbf{u}(\mathbf{C})) = \int_{\Gamma_1} \mathbf{t} \cdot \mathbf{u}(\mathbf{C}) \, da \quad (42)$$

under the isoperimetric condition:

$$\int_{\Omega} \operatorname{tr} \mathbf{C} \, dx = \int (2k + 4\mu) \, dx \leq \Lambda, \quad (43)$$

where the kinematically admissible vector field

$$\mathbf{u} = \mathbf{u}(\mathbf{C}) \quad (44)$$

is a solution to the following equilibrium equation:

$$\forall \mathbf{v} \in V(\Omega) \quad \int_{\Omega} \boldsymbol{\tau} \cdot \boldsymbol{\varepsilon}(\mathbf{v}) \, dx = \int_{\Gamma_1} \mathbf{t} \cdot \mathbf{v} \, da. \quad (45)$$

By $\boldsymbol{\varepsilon}(\mathbf{u})$ and $V(\Omega)$, we denote the strain tensor and the space of all kinematically admissible displacements, respectively. In other words, $\mathbf{v} \in V(\Omega)$ is the displacement field vanishing on a given boundary fragment $\Gamma_2 \subset \partial\Omega$. This also means that the stress tensor

$$\boldsymbol{\sigma}(\mathbf{u}) = \mathbf{C}\boldsymbol{\varepsilon}(\mathbf{u}) \in \Sigma(\Omega) \quad (46)$$

satisfies the equilibrium equation, where $\Sigma(\Omega)$ denotes the set of statically permissible stresses, i.e., the set of all symmetric second-order tensors satisfying Eq. (45). After using Castigliano's theorem, one can derive the following topology optimization problem for the elastic body Ω with the isoperimetric condition (43):

$$\Phi^* = \min_{\boldsymbol{\tau} \in \Sigma(\Omega)} \Phi(\boldsymbol{\tau}), \quad \boldsymbol{\tau}^* = \arg \min_{\boldsymbol{\tau} \in \Sigma(\Omega)} \Phi(\boldsymbol{\tau}) \in \Sigma(\Omega), \quad (47)$$

where

$$\Phi : \Sigma(\Omega) \rightarrow R, \quad \forall \boldsymbol{\tau} \in \Sigma(\Omega), \quad \Phi(\boldsymbol{\tau}) = \int_{\Omega} |\boldsymbol{\tau}| \, dx \quad (48)$$

is the objective function, not involving the design scalar fields $k(x)$, $\mu(x)$, $x \in \Omega$. In the case of 2D problem, the integrand function is the norm defined as follows:

$$|\boldsymbol{\tau}| = \frac{\sqrt{2}}{2} |\operatorname{tr} \boldsymbol{\tau}| + \sqrt{2} \|\operatorname{dev} \boldsymbol{\tau}\|, \quad (49)$$

where $|\operatorname{tr} \boldsymbol{\tau}|$, $\|\operatorname{dev} \boldsymbol{\tau}\|$ on the right-hand side of Eq. (49) represent the absolute value of the trace and the standard Euclidean norm of the deviator of $\boldsymbol{\tau}$, respectively.

Once the minimizer

$$\boldsymbol{\tau}^* \in \Sigma(\Omega) \quad (50)$$

of Φ is found, then the fields

$$k^*(x) = \frac{\frac{\Lambda}{2\sqrt{2}} |\operatorname{tr} \boldsymbol{\tau}^*(x)|}{\int_{\Omega} |\boldsymbol{\tau}^*| \, dx}, \quad \mu^*(x) = \frac{\frac{\Lambda}{2\sqrt{2}} \|\operatorname{dev} \boldsymbol{\tau}^*(x)\|}{\int_{\Omega} |\boldsymbol{\tau}^*| \, dx}, \quad (51)$$

form the solution to the topology minimization problem for two-dimensional bodies, as described, e.g., in [20], where a detailed description and summary of many papers concerning topology optimization of elastic bodies in the stress version can be found.

It is obvious that any numerical simulation must be preceded by the interpolation of statically allowable stresses $\boldsymbol{\tau} \in \Sigma(\Omega)$ in order to convert the infinite-dimensional problem into a finite-dimensional problem, resulting in linear equations of the form:

$$\mathbf{B} \mathbf{T} = \mathbf{Q}, \quad (52)$$

where \mathbf{B} is the rectangular matrix, and \mathbf{Q} , $\mathbf{T} = \mathbf{T}(\boldsymbol{\alpha})$ are the vectors of nodal forces and unknown nodal stress parameters, respectively, depending on vectors

$$\boldsymbol{\alpha} = (\alpha_1, \dots, \alpha_r) \in R^r, \quad r = \dim \ker \mathbf{B} \quad (53)$$

that span the kernel of the equilibrium matrix \mathbf{B} , defining the interpolations of stresses. In the paper [21], the interpolation of the stress field components is described in detail, and the numerical calculations are carried out by introducing an additional plasticity condition for statically admissible stress fields $\boldsymbol{\tau} \in \Sigma(\Omega)$:

$$\forall x \in \Omega, \quad \gamma(\boldsymbol{\tau}(x)) \leq \sigma_0, \quad (54)$$

where σ_0 represents the plastic limit corresponding to the tensile test, and

$$\gamma(\boldsymbol{\sigma}) = \sqrt{\frac{1}{2} \left(\frac{1}{\sqrt{2}} \operatorname{tr} \boldsymbol{\sigma} \right)^2 + \frac{3}{2} \|\operatorname{dev} \boldsymbol{\sigma}\|^2} \quad (55)$$

for 2D problem. The algorithm taking into account the yield condition (54), together with the presentation of numerous numerical examples, is described in detail in [21].

4. Case studies

The results and comments in examples 4.1–4.5 below are given exclusively for truss structures. However, Subsec. 4.6 additionally presents the results of topology optimization for a 2D elastic body Ω , which is loaded statically using

the IMD method. In this case, the objective function – compliance (42) – is equivalent to the total potential energy for trusses, assuming no kinematic loads (i.e., $\mathbf{U} = \mathbf{0}$ in formulas (15) and (37)). The aim is to highlight the occurrence of almost identical properties between both objective functions, as well as the resulting challenges in interpreting the results of optimal solutions.

The singular value decomposition (SVD) algorithm, together with routines implementing non-linear mathematical programming algorithms such as Fletcher–Reeves (FR), Polak–Ribiere (PR), or Broyden–Fletcher–Goldfarb–Shanno (BFGS) [22], was used to find the statically admissible representation and the optimal solution, respectively. The Young modulus E and the initial cross-sectional area A_k^{init} , $k = 1, 2, \dots, e$, of each member of the optimized truss (whether planar or spatial) are equal to $E = 7.2 \cdot 10^6$ N/cm² and 1.0 cm², respectively. In almost all examples, the limitation Λ of not exceeding the allowable material resources in isoperimetric condition is equal to

$$\Lambda = \sum_{k=1}^e EA_k^{\text{init}} l_k \text{ [N} \cdot \text{cm]}, \quad (56)$$

where l_k , $k = 1, 2, \dots, e$ are the lengths of the truss members. Only in example 4.5 (hangar roof) are the optimization results for the truss shell structure shown with Λ calculated using (56) and additionally according to $\widehat{\Lambda}$, where

$$\widehat{\Lambda} = 4 \cdot \Lambda = 4 \cdot \sum_{k=1}^e EA_k^{\text{init}} l_k \text{ [N} \cdot \text{cm]} \quad (57)$$

in order to investigate the influence of the isoperimetric condition (3), (4) on the final compliance optimization result.

In selected examples where the kernel dimension $r = \dim \ker \overline{\mathbf{B}}^T$ is equal to 2, the graph of the minimized functional $J(\boldsymbol{\alpha})$ is shown in order to reveal some of its features, which have a significant impact on both the uniqueness and numerical efficiency of finding its optimal value $J^* = \frac{F^*}{2}$. Red and blue colors indicate members in tension and compression states, respectively. When green stars appear in the figures, they indicate truss supports. Several figures use the notation α_0 , α_1 instead of the α_1 , α_2 used in the text, as the indexing in the Python program used for visualizing these graphs starts from 0 rather than 1.

4.1. Two-member truss

As a first example, consider a symmetrical, two-member truss structure that is pin-supported at all its three nodes, see Fig. 2a. The lengths of the projections of the structure on the horizontal and vertical axis are 200 cm and 50 cm, respectively. Therefore, the limitation Λ in the isoperimetric condition is given by:

$$\sum_{k=1}^2 EA_k^{\text{init}} l_k = \Lambda = 1.60997 \cdot 10^9 \text{ [N} \cdot \text{cm]}.$$

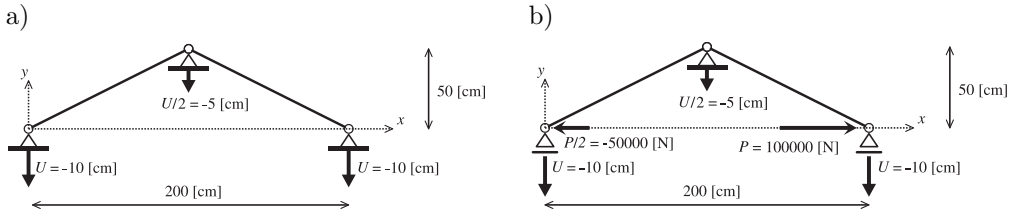


FIG. 2. Two member structure, pin-supported at three nodes: a) twice statically indeterminate (all six degrees of freedom of the three nodes are considered). The structure is loaded kinematically by three vertical displacements in the downward direction U , $U/2$, U for the left, middle and right node, respectively, b) statically determinate (with the possibility of the independent displacements in the horizontal direction for the left and right nodes); the structure is loaded kinematically in the same way as in case a, but additionally, it is loaded with two horizontal forces with opposite directions and different values $P/2$ and P are applied to the left and right nodes, respectively.

All three supports move vertically downward: the lower left and right supports move by a value $U = 10$ cm, and the upper middle one moves by the $U/2 = 5$ cm. The kernel dimension r in this example is equal to 2, which makes it possible to draw a graph of the minimized functional $2J(\alpha)$, $\alpha = (\alpha_1, \alpha_2) \in R^2$, as shown in Fig. 3. As clearly visible, the graph of the functional $J(\alpha)$ has the

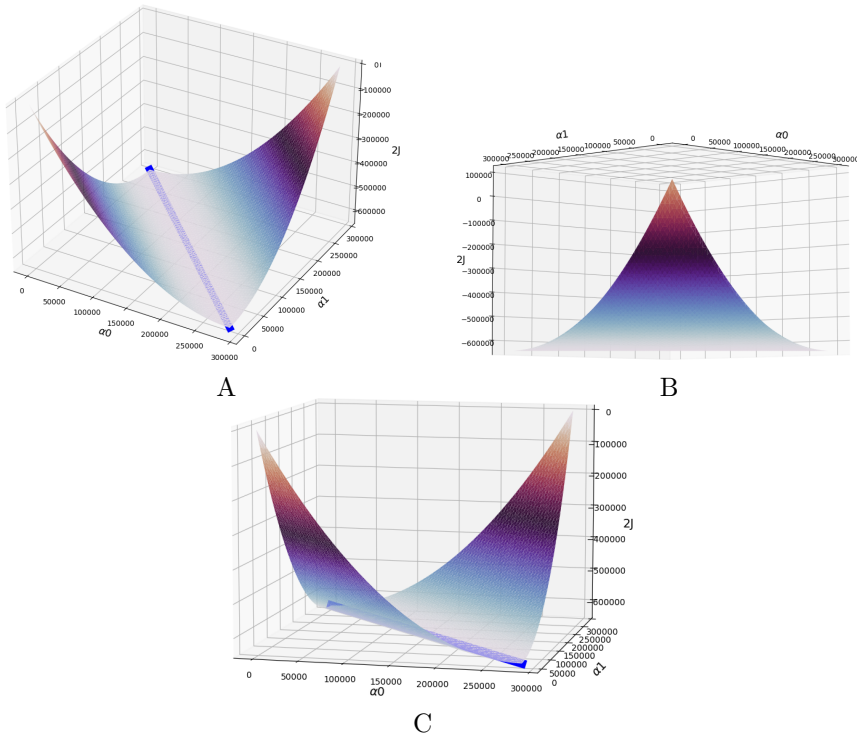


FIG. 3. Three-member structure from Fig. 2a: two different views of the graph of the $2J(\alpha)$ functional.

shape of a long and flat valley. At each point $\alpha \in R^r$ located along the section marked in blue, the value of the functional reaches the minimum global value $J^* = \frac{-643988}{2} = -321994$ [N · cm]. In Fig. 4, five of the infinitely many alternative solutions (i.e., optimal cross-sectional areas A_k^* , $k = 1, 2$) of this truss are shown. In each case, the isoperimetric condition is satisfied equally. When both members have different lengths and the six independent horizontal and vertical displacements of each support are different, the graphs of the functional $J(\alpha)$, although similar to the one in Fig. 3, usually have one global minimum. However, this minimum often lies at the end of a very long and almost flat valley. This explains the numerical difficulties encountered in finding the minima that appeared during numerical tests carried out on truss structures, where it is not always possible to visualize the objective function.

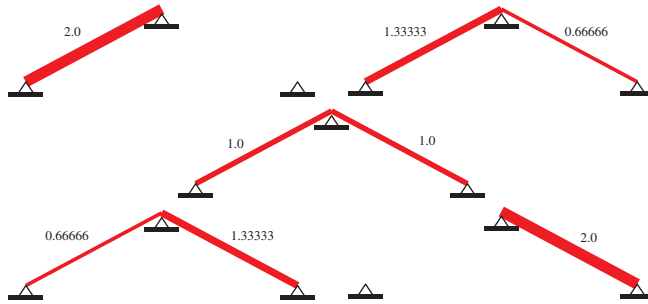


FIG. 4. Two-member structure: five various alternative topology optimization solutions – optimal cross-sectional area A_k^* , $k = 1, 2$ cm² for the truss from Fig. 2a.

As a second example, consider the same two-member truss structure shown in Fig. 2b. This time, the truss is statically determinate (left and right nodes are free to move horizontally). In addition to the same kinematic load as in the previous case, it is also loaded with horizontal forces $P/2$ and P ($|P| = 100\,000$ N), applied in opposite directions to the left and right nodes, respectively – see Fig. 2b. It is well known that, within the geometrically linear theory of rods, no kinematic, distortion and thermal loads (in particular, support displacements) induce a state of stress in a statically determinate structure. Therefore, the topology optimization result is only influenced by the static load. In this case, the forces in the truss members, uniquely determined from the equilibrium equations, define the asymmetrical, unique optimal cross-sections, as shown in Fig. 5.

It is worth emphasizing here that, within the geometrically linear theory of member structures, the displacements of nodes in an optimal truss loaded statically and kinematically at the same time are the superposition of the displacements of the optimal truss loaded only statically and the displacements of the optimal truss loaded only kinematically. Of course, the principle of superposition also applies to the internal forces in members, and reactions at outer



FIG. 5. Two-member structure. Unique topology optimization solution for the truss from Fig. 2b.

supports. In our particular case, the unknown horizontal displacements (measured in cm) of the left, middle and right nodes caused only by the horizontal displacements of all three nodes can be relatively easily calculated (e.g., based on the displacement plan) and are equal to:

$$+2.5, 0.0, \text{ and } -2.5,$$

respectively (assuming positive directions for displacements in the horizontal and vertical directions, to the right and up, respectively). The known vertical displacements are, of course:

$$-10.0, -5.0, \text{ and } -10.0,$$

respectively. The unknown horizontal displacements of the left, middle and right nodes caused only by the static load were found using the FEM after optimization and are equal to:

$$-1.45577, 0.0, \text{ and } +1.45577,$$

respectively. All known vertical displacements, of course, remain equal to 0.0 cm. The superposition of all above-found displacements gives:

$$2.5 - 1.45577 = +1.04423, 0.0 + 0.0 = 0.0, \text{ and } -2.5 + 1.45577 = -1.04423$$

in horizontal directions and

$$-10.0 + 0.0 = -10.0, -5.0 + 0.0 = -5.0, \text{ and } -10.0 + 0.0 = -10.0$$

in vertical directions, respectively. Exactly the same values of all nodal displacements were obtained after topology optimization in the case of static and kinematic loads applied simultaneously to the truss nodes. It is also worth noting that, in this particular task, despite the optimal solution being asymmetric (see Fig. 5) (because the load is not symmetrical), the final optimal horizontal displacements of the supports are symmetrical. The optimal values J^* of the functional for pure kinematic and pure static loading are equal to 0 and 109 183 N·cm, respectively, and their superposition is, of course, not equal to the optimal value $J^* = -265 817$ N·cm for kinematic and static loadings applied simultaneously. It may also be worth mentioning that any displacements of supports causing rigid rotation of any elastic body within the limits allowed by geometrically linear theories of structures also do not cause any deformations.

4.2. Four-member truss

The upper right support node of the twice statically indeterminate truss shown in Fig. 6 is subject to displacement $U = 1.4142$ cm along member 3, while a vertical force $P = 200\,000$ N is applied to the inner node. The value Λ in the isoperimetric condition is, in this case, equal to $3.476467530 \cdot 10^9$ N · cm. The kernel dimension r is equal to 2, which makes it possible to draw a graph of the minimized functional $J(\alpha)$, revealing a very important feature that sometimes appears not only in topology optimization of truss structures but also in the topology optimization of any two- or three-dimension elastic bodies.

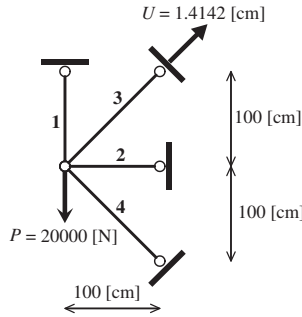


FIG. 6. Dimensions of the four-member truss. The absolute values of nodal static and kinematic loading are $P = 2.0 \cdot 10^5$ N and $U = 1.4142$ cm, respectively.

In this example (similarly to the first one presented in Fig. 2a), the convex functional J seems to have (with numerical accuracy up to six decimal places) infinitely many global minima $\alpha^* \in R^r$ located on the blue line – see Fig. 7. At each ten points $\alpha^* = (\alpha_1^*, \alpha_2^*) \in R^r$, regularly spaced on the blue segment shown in Fig. 7 the value of the functional $J^* = 52\,353.2/2 = 26\,176.6$ [N · cm] is the same for all these points. In Table 1, ten optimal member cross-sections A_k^* , $k = 1, 2, 3, 4$ [in cm^2] for this ten optimal solutions are presented. In Fig. 8, ten optimal trusses are shown in the same order as in Table 1, while maintaining

TABLE 1. Cross-sectional areas of truss members for ten different points $\alpha^* = (\alpha_1^*, \alpha_2^*) \in R^r$ at which the functional J reaches the same (at least numerically) optimal value $J^* = 26\,176.6$ N · cm, listed in the order from the upper right to the lower left point located on the blue section visible in the third view of Fig. 7.

$(\alpha_1^*, \alpha_2^*)/10^4$	$(-3.60, 10.34)$	$(6.74, 0)$
A_1^* [cm^2]	1.74	1.63	1.52	1.40	1.29	1.18	1.07	0.95	0.84	0.73
A_2^* [cm^2]	1.01	0.90	0.79	0.68	0.56	0.45	0.34	0.22	0.11	0.00
A_3^* [cm^2]	1.45	1.45	1.45	1.45	1.45	1.45	1.45	1.45	1.45	1.45
A_4^* [cm^2]	0.00	0.17	0.33	0.49	0.65	0.81	0.97	1.13	1.29	1.45

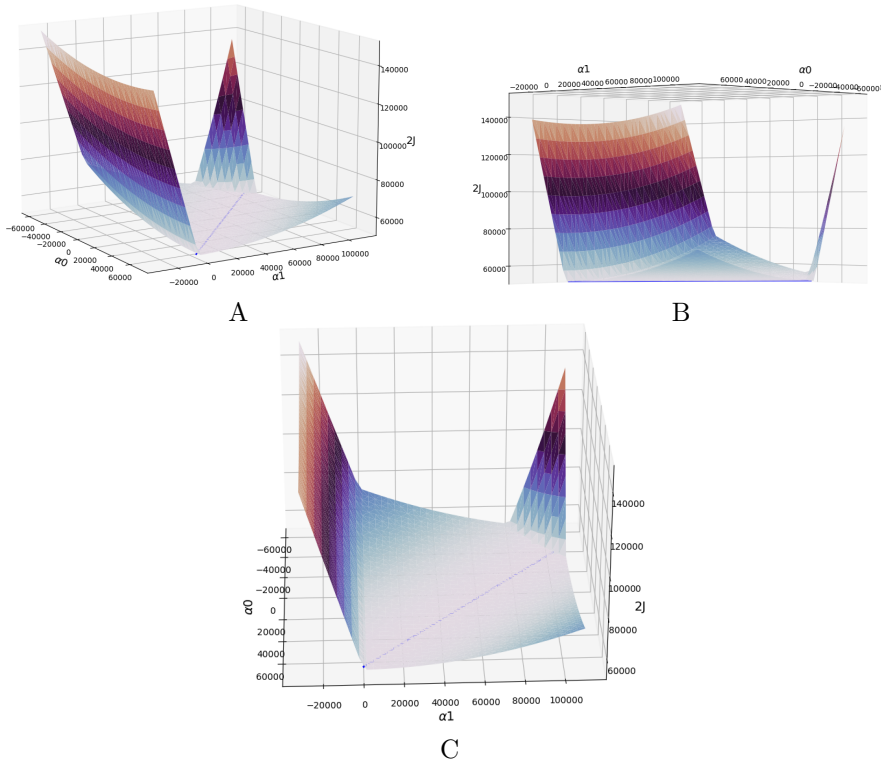


FIG. 7. Three different views of the graph of the $2J(\alpha)$ functional for the four-member truss shown in Fig. 6, loaded simultaneously statically and kinematically.

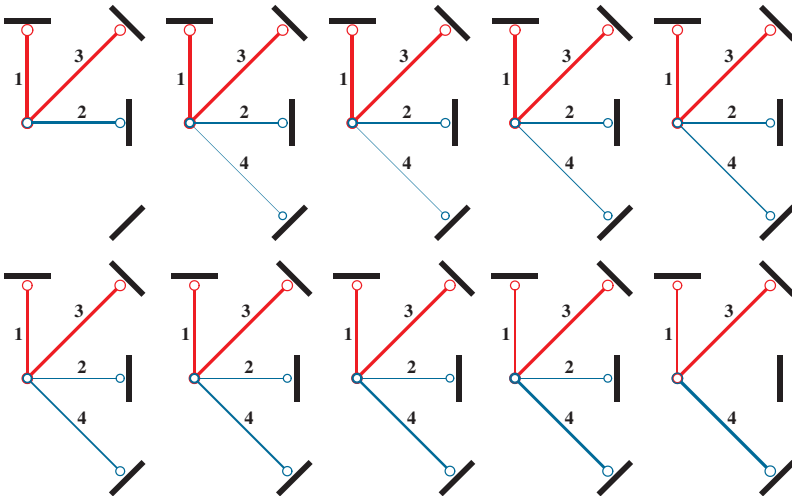


FIG. 8. Optimal truss members (red/blue – tension/compression) for points $\alpha^* = (\alpha_1^*, \alpha_2^*) \in R^T$ from Table 1 for which the functional J reaches the same (at least numerically) optimal value $J^* = 26\,176.6\text{ N} \cdot \text{cm}$.

the same scale of line thicknesses corresponding to the cross-sectional areas of the members. In each of the 10 optimal solutions, the isoperimetric condition was always met ‘equally’, i.e.,

$$\sum_{k=1}^e EA_k^* l_k = \Lambda.$$

Based on many other numerical simulations for optimal topologies according to the IMD, method carried out for both for truss structures and two/three-dimensional elastic bodies, the existence of flat and long valleys characterizing the ‘graph’ of the functional J in R^r ($r \gg 2$) cannot be ruled out in subdomains where the global minimum is reached. In the general case (also when we are dealing with only static loads), the optimal topology of a truss structure or, alternatively, the optimal distribution of elastic moduli in a two- or three-dimensional body, may sometimes depend on the starting point $\alpha \in R^r$, which defines the initial set of statically admissible forces or stress fields. However, in many numerical calculations, even if different optimal topologies were obtained for different starting points α , the optimal values of the minimized functional J (or its equivalent in 2D/3D continuum mechanics) are almost always identical (with, of course, assumed numerical accuracy).

The next two numerical results for special cases of only static or only kinematic loading are shown in Figs. 9 and 10, and Table 2.

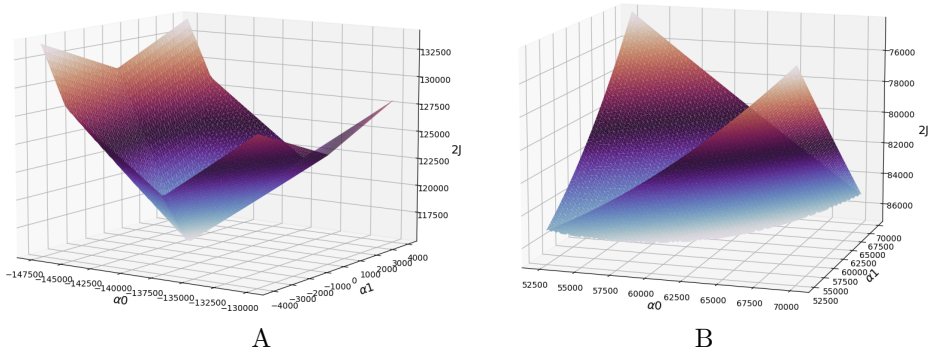


FIG. 9. Two views of the graph of the objective function in the case of only static or only kinematic loading of the truss shown in Fig. 6, respectively.

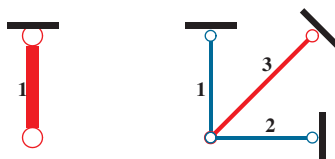


FIG. 10. Optimal truss members (red/blue – tension/compression) for points $\alpha^* = (\alpha_1^*, \alpha_2^*)$ from Table 2.

TABLE 2. Optimal points α^* , optimal values $J(\alpha^*)$, and optimal cross-sectional areas of truss members in the case of only static or only kinematic loading, shown in second and third columns, respectively.

$\alpha^* = (\alpha_1^*, \alpha_2^*)$	(-141 421.0, 0.0)	(61 455.8, 61 455.8)
$J(\alpha^*)$	57 529.5	-43 455.8
$A_1^* [\text{cm}^2]$	4.83	1.21
$A_2^* [\text{cm}^2]$	0.00	1.21
$A_3^* [\text{cm}^2]$	0.00	1.71
$A_4^* [\text{cm}^2]$	0.00	0.00

This example, together with the objective function graphs in Fig. 9, clearly indicates that in both of these different loading cases, the objective function achieves exactly one global minimum.

4.3. Eight-member truss

The eight-member truss is supported at the left and right nodes, while the lower and upper nodes can move freely in the horizontal direction. The lengths of all horizontal and vertical members are 100 cm. Two pairs of forces parallel to each other and with opposite directions applied to the truss at the two middle nodes and at the lower and upper nodes, respectively. The absolute values of all forces are equal to $|P| = 200\,000$ N. Both variants of the static load are shown in Fig. 11. Regardless of the static load, the leftmost and rightmost nodes move by $U = 1$ cm or $U = 3$ cm in the horizontal direction to the left and right, respectively.

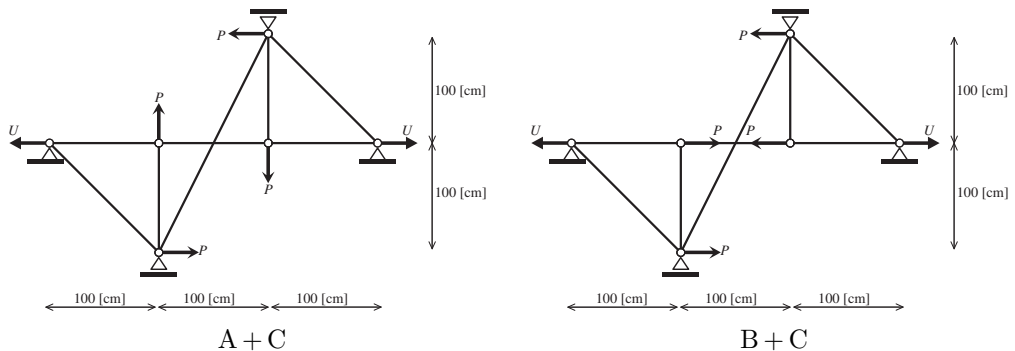


FIG. 11. Two variants: A and B of a static eight-member load applied to the truss nodes with force pairs P , together with an independent variant C of kinematic stretching load U applied to the leftmost and rightmost nodes.

In Fig. 12, the optimal truss topology is shown for variant C of kinematical loading for $U = 1$ cm. Optimal value: $J^* = 322\,064/2 = 161\,032$ [N · cm], op-

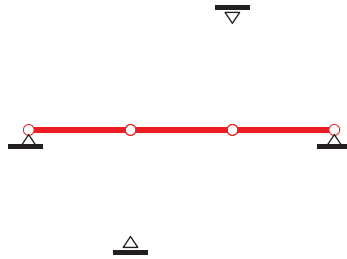


FIG. 12. Variant C, optimal eight-member truss structure.

timal cross-sections of the three horizontal red members: 3.35483 cm^2 , and all other members disappear because the areas of their optimal cross-sections are equal to 0.

In Fig. 13, optimal truss topology is shown for load variant A. Optimal value $J^* = 1.99 \cdot 10^6 / 2 = 0.99 \cdot 10^6 \text{ [N} \cdot \text{cm]}$, optimal cross-sections of the two vertical red members: 1.67742 cm^2 , and optimal cross-sections of the two red skew members: 2.37222 cm^2 . The remaining members disappear.

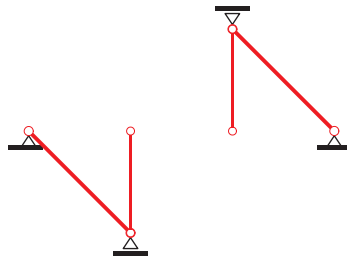


FIG. 13. Optimal eight-member truss structure (red – tension) for variant A.

Then, a solution to the optimization problem was sought for both of the above variants, A and C: simultaneous static and kinematic load. The optimal value of $J^* = 1.19 \cdot \frac{10^6}{2} = 0.6 \cdot 10^6 \text{ [N} \cdot \text{cm]}$ ($< 0.99 \cdot 10^6$), was smaller than in the previous case; however, the optimal cross-sections of the two red horizontal members and optimal cross-sections of the two red skew members were numerically almost equal to each other. Since it is also possible to plot the objective function in this example, it turns out that it has a very similar shape to that of the previous four-member truss problem: a long, however, not a flat but rather very narrow valley – see Fig. 14. This explains the significant numerical difficulties that, in this case, resulted in an unconvincing result for the final truss optimization (practically identical to that in the case of only static loading).

In the second variant of this case, the displacement value was increased from $U = 1 \text{ cm}$ to $U = 3 \text{ cm}$. The calculations were repeated, and this time the following results were obtained: optimal value $J^* = 498\,575 / 2 = 249\,287.5 \text{ [N} \cdot \text{cm]}$,

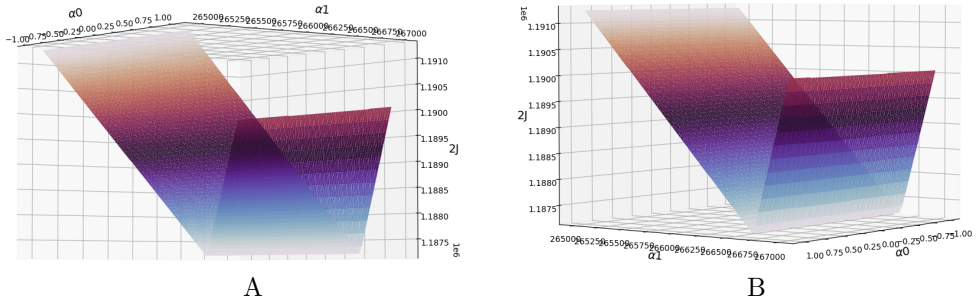


FIG. 14. Two views of the graph of the functional in the case of variants A and C for kinematic displacement of the left- and right-most nodes equal to $U = 1.0$ cm.

optimal cross-sections of the two red vertical members: 1.38889 cm^2 , optimal cross-sections of the three red horizontal members: 0.577054 cm^2 , and optimal cross-sections of the two red skew members: 1.96419 cm^2 , see Fig. 15.

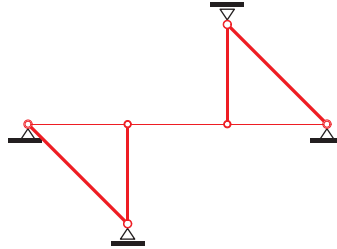


FIG. 15. Optimal eight-member truss structure (red – tension) for variants A and C for kinematic displacement of leftmost and rightmost nodes increased from 1 to 3 cm.

This time, by comparing the objective function graph shown in Fig. 16 with the previous one, we can clearly see the point of the global minimum, which is easy to locate in numerical calculations.

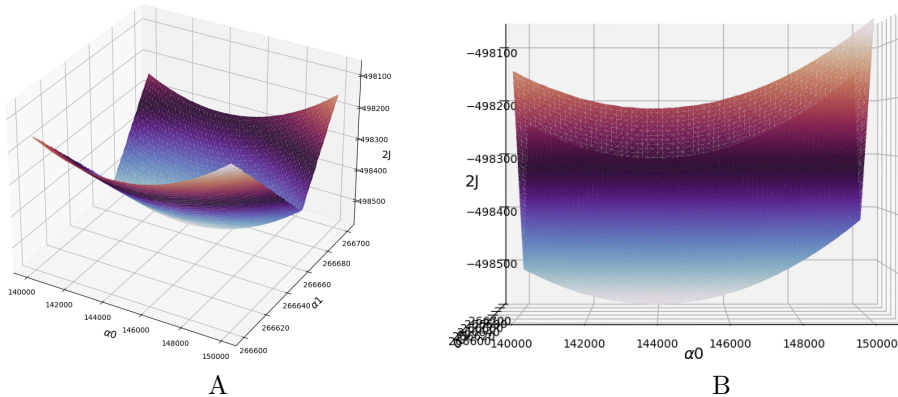


FIG. 16. Two graphs of the functional in the case of A and C variants for kinematic displacement of the leftmost and rightmost nodes increased from $U = 1$ cm to $U = 3$ cm.

Similarly to variants A and A + C, a simulation of the search for the optimal truss topology was carried out for variants B and B + C for $U = 1$ cm. The following results (see Fig. 17) were obtained for variant B: optimal value $J^* = 1.38 \cdot 10^6 / 2 = 0.69 \cdot 10^6$ [N · cm], optimal cross-section of the one horizontal blue member: 2.0129 cm², optimal cross-sections of the two red skew members: 2.84667 cm². For variant B + C: optimal value $J^* = 387\,184 / 2 = 193\,592$ [N · cm], optimal cross-sections of the two red horizontal members: 1.67742 cm², and optimal cross-sections of the two red skew members: 2.37222 cm².

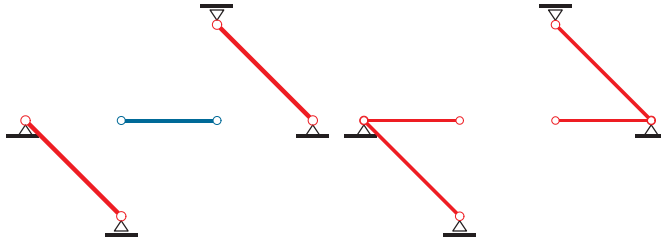


FIG. 17. Optimal eight-member truss structure (red/blue – tension/compression) for variant B and variant B + C for $U = 1$ cm.

The optimal solutions presented in Fig. 17 may be somewhat surprising due to the obvious discontinuity in the connections between the members and their suspension – as if the structure were in a state of weightlessness. However, let us remember that in the presented optimization method we allow for the possibility of removing selected bars, while ensuring that all equilibrium equations of the structure's elements are always satisfied under a given load (the weight of the members, which, according to the truss theory could only be indirectly taken into account via equivalent loads at the nodes, is omitted in this example). Therefore, the optimal structure, especially in the case of no nodal loads or very specific nodal loads (aside from the reactions at the support nodes, of course) may appear as shown in Fig. 17, while still meeting all the imposed constraints. The disappearance of members in displacement-oriented static methods, where the stiffness matrix plays a key role, is, of course, not permissible for obtaining optimal solutions like those in Fig. 17, and at most, anticipating the possibility of evolving the algorithm in such a direction that members may ‘want to disappear’ during the optimization process, additional constraints are usually introduced, e.g., to limit the minimum permissible cross-sections of members, to effectively protect against the occurrence of stiffness matrix singularities. However, in the case of stress-oriented static methods, where the key role is played not by the stiffness matrix, but by a rectangular geometric equilibrium matrix (usually with more columns than rows), it is possible to satisfy all equations in such cases, even when members (which transfer internal forces) disappear. This illustrates, in a sense, the superiority of stress-based methods

over displacement-based methods, in the context of their use in the optimization of structural topology.

4.4. Fourteen-member truss

The 14-member truss is supported at the two upper nodes and is loaded statically with vertical forces applied to two right nodes with $|P| = 1.0 \cdot 10^4$ N (see Fig. 18).

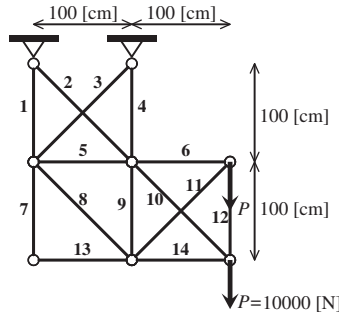


FIG. 18. The dimensions of the 14-member truss with two vertical forces P applied to the two right nodes.

The random selection of the design parameter, which initializes the process of searching for the minimum of the J functional, determines the final value of the α^* minimizer. As a result, the calculated optimal cross-sectional areas of the members A_k^* , $k = 1, \dots, 14$, differ practically after each program run. However, the optimal values of $2J^*$ are identical and equal to $38\,112$ N · cm, as confirmed by the graph of the $2J$ functional shown in Fig. 19.

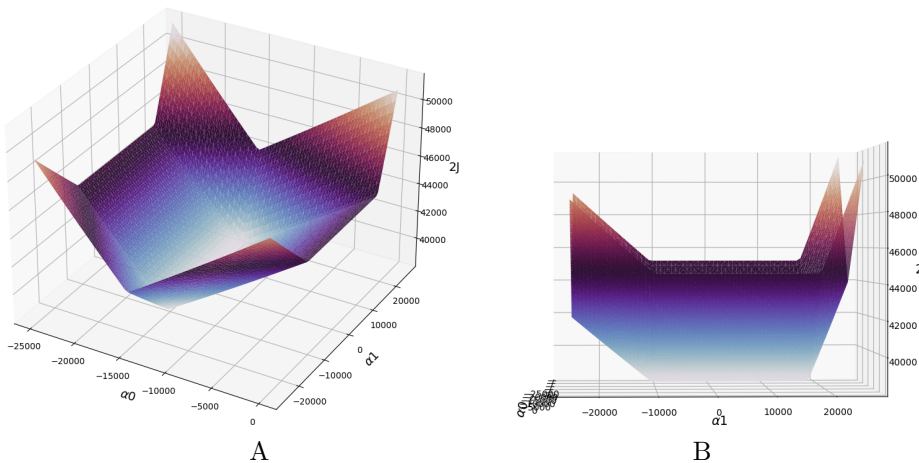


FIG. 19. Two views of the graph of the functional for 14-member truss with two vertical forces P applied to the two right nodes.

cross-sections of the bars that were not removed in the optimization process can only apply to the six remaining, which form something like a rigid plate in its lower-right area. This may explain why some of the cross-sectional areas in the three presented designs are different, while others always remain unchanged.

In cases where we deal with hundreds or even thousands of members in lattice structures, it is of course not possible to visualize the objective function J . Doubts about the correctness of finding the global minimum $\alpha^* \in R^r$ ($r > 2$) of the functional J are not easy to resolve, especially if different optimal distributions A_k^* , $k = 1, \dots, e$, of the cross-sections of the members are accompanied by different optimal values $J^* = J(\alpha^*)$, which, however, are within the limits of numerical calculation accuracy. To address this, verification and control calculations require repeating the optimization process for any, for example, randomly generated, initial values α^{init} of the design parameter α . As shown in many of the examples cited above, this often results in obtaining slightly or significantly different optimal solutions α^* , with identical or only slightly different optimal numerical values of J^* .

4.5. Hangar roof in the shape of a structural shell

We will now present the results of the topology optimization of a structural shell subjected to kinematic loading and simultaneous kinematic and static loading. The shell spans a square with dimensions $L_x \times L_y = 1500 \times 1500$ cm, and its equation in the Cartesian coordinate system is as follows: $z = -\xi \left(\frac{x}{L}\right)^2$, where $L = 40$ cm, and $\xi = 1$ cm, see Fig. 21. The shell is pin-supported (non-sliding) at all boundary nodes lying on both edges parallel to the Oy -axis. These edges experience linear displacements along the Oy -axis in such a way that, in the first case (see Fig. 21A, the values of the corner vertical displacements are equal to $U = -2$ cm, while the displacements of the nodes with coordinates $\left(0, \pm \frac{L_y}{2}\right)$ are equal to zero. In the second case (see Fig. 21B, the values of the four corner displacements are equal to zero, and the vertical settlement of both nodes with coordinates $\left(0, \pm \frac{L_y}{2}\right)$ is $U = -2$ cm. In the case of additional static loading, a horizontal force $Q_y = 5000$ N and a vertical force $Q_z = -10\,000$ N were applied to each shell node. The value of the resultant force $|P|$ at each node is therefore $|P| = \sqrt{Q_y^2 + Q_z^2} \approx 11\,180$ N. The density of a regular mesh of members, with diagonal members intersecting at the middle of the square modules, depends on the number of I , J columns and rows of nodes, respectively. Two variants of the grid density were adopted: $I \times J = 5 \times 5$ and $I \times J = 15 \times 15$ (see Fig. 21C) in order to reveal their influence on the shell's compliance, and, indirectly, on the magnitude of node displacements. This influence is also dependent on the value of the Λ parameter appearing in the isoperimetric conditions (3) and (4).

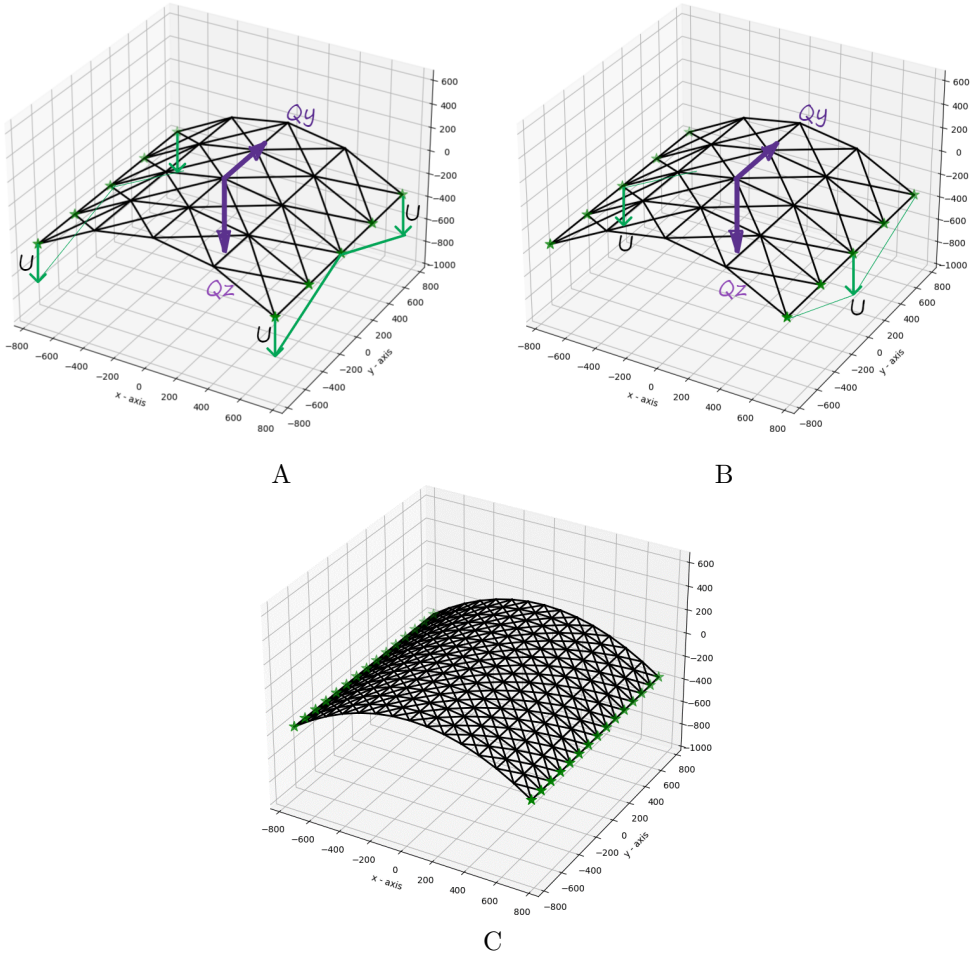


FIG. 21. Both kinematic (U) loading versions: A or B without or with additional static load (Q_y, Q_z) for a truss shell with a mesh density $I \times J = 5 \times 5$, respectively; C – truss shell with a higher mesh density $I \times J = 15 \times 15$ loaded in accordance with variant A or B.

In order to better interpret the results, the optimal layouts presented below (see Tables 4 and 5, and Figs. 22 and 23) are shown in a deformed configuration, revealing the very high sensitivity of the analysed structural shell to the density of the mesh of lattice members. This is manifested by significantly increased displacements of many nodes, which exceeds allowable values in the linear-geometric static analysis. It should be emphasized here that, as a result of the topology optimization using the stress method (based on Castigliano's theorem), a large number of members in the original truss usually disappear after optimization. This occurs because the algorithm is by definition not sensitive to the disappearance of members in the optimal topology (equilibrium

TABLE 4. Six $\boxed{1} \div \boxed{6}$ optimal values $F^* = 2J^*$ [N·cm] of the compliance F , along with the minimum A_{\min}^* , q_{\min}^* and maximum A_{\max}^* , q_{\max}^* ([cm²], [cm]) values of the optimal cross-sectional areas A_k^* for lattice members and the optimal nodal displacements q_i^* . Results are presented for versions A and B of kinematic loading only for shells with densities 5×5 , 15×15 for Λ and 15×15 for $\hat{\Lambda} = 4\Lambda$ [N/cm²] values in the isoperimetric condition.

Mesh density Λ or $\hat{\Lambda}$	Variant A for only U	Variant B for only U
5×5 , $\Lambda = 2.45 \cdot 10^{11}$	$F^* = -66\,784$ $\boxed{1}$ $A_{\min}^* = 0$, $A_{\max}^* = 6.38$, $q_{\min}^* = -2.82$, $q_{\max}^* = 0.65$	$F^* = -67\,281$ $\boxed{2}$ $A_{\min}^* = 0$, $A_{\max}^* = 6.43$, $q_{\min}^* = -2.47$, $q_{\max}^* = 0.65$
15×15 , $\Lambda = 8.02 \cdot 10^{11}$	$F^* = -246\,482$ $\boxed{3}$ $A_{\min}^* = 0$, $A_{\max}^* = 48.65$, $q_{\min}^* = -12.20$, $q_{\max}^* = 9.01$	$F^* = -248\,002$ $\boxed{4}$ $A_{\min}^* = 0$, $A_{\max}^* = 48.81$, $q_{\min}^* = -10.80$, $q_{\max}^* = 10.20$
15×15 , $\hat{\Lambda} = 3.21 \cdot 10^{12}$	$F^* = -977\,144$ $\boxed{5}$ $A_{\min}^* = 0$, $A_{\max}^* = 192.87$, $q_{\min}^* = -12.01$, $q_{\max}^* = 8.99$	$F^* = -982\,080$ $\boxed{6}$ $A_{\min}^* = 0$, $A_{\max}^* = 193.71$, $q_{\min}^* = -10.60$, $q_{\max}^* = 9.63$

TABLE 5. Six $\boxed{1'} \div \boxed{6'}$ optimal values $F^* = 2J^*$ [N·cm] of the compliance F , along with the minimum A_{\min}^* , q_{\min}^* and maximum A_{\max}^* , q_{\max}^* ([cm²], [cm]) values of the optimal cross-sectional areas A_k^* for lattice members and the optimal nodal displacements q_i^* . Results are presented for versions A and B of simultaneous kinematic and static loading, for shells with densities of 5×5 , 15×15 for Λ and 15×15 for $\hat{\Lambda} = 4\Lambda$ [N/cm²] values in the isoperimetric condition (3) and (4).

Mesh density Λ or $\hat{\Lambda}$	Variant A for U and Q_y , Q_z	Variant B for U and Q_y , Q_z
5×5 , $\Lambda = 2.45 \cdot 10^{11}$	$F^* = 602\,350$ $\boxed{1'}$ $A_{\min}^* = 0$, $A_{\max}^* = 4.02$, $q_{\min}^* = -4.36$, $q_{\max}^* = 2.24$	$F^* = 420\,700$ $\boxed{2'}$ $A_{\min}^* = 0$, $A_{\max}^* = 4.32$, $q_{\min}^* = -4.59$, $q_{\max}^* = 1.40$
15×15 , $\Lambda = 8.02 \cdot 10^{11}$	$F^* = 1.4 \cdot 10^7$ $\boxed{3'}$ $A_{\min}^* = 0$, $A_{\max}^* = 4.98$, $q_{\min}^* = -45.8$, $q_{\max}^* = 49.08$	$F^* = 1.3 \cdot 10^7$ $\boxed{4'}$ $A_{\min}^* = 0$, $A_{\max}^* = 4.98$, $q_{\min}^* = -51.91$, $q_{\max}^* = 52.48$
15×15 , $\hat{\Lambda} = 3.21 \cdot 10^{12}$	$F^* = 6.6 \cdot 10^6$ $\boxed{5'}$ $A_{\min}^* = 0$, $A_{\max}^* = 24.03$, $q_{\min}^* = -12.49$, $q_{\max}^* = 11.80$	$F^* = 5.9 \cdot 10^6$ $\boxed{6'}$ $A_{\min}^* = 0$, $A_{\max}^* = 20.57$, $q_{\min}^* = -19.01$, $q_{\max}^* = 21.64$

equations are not defined by the classical stiffness matrix as in FEM). Therefore, reproducing the displacement state in the optimal truss quite often requires some additional procedures, such as replacing the removed members (as a result of optimization) with members having very small cross-sectional areas, e.g., on the order of $1.0 \cdot 10^{-12}$ cm². This depends on how the procedure for finding numerical solutions to systems of linear equations (with a given stiffness matrix and the vector of nodal displacements as unknowns) addresses the problem of

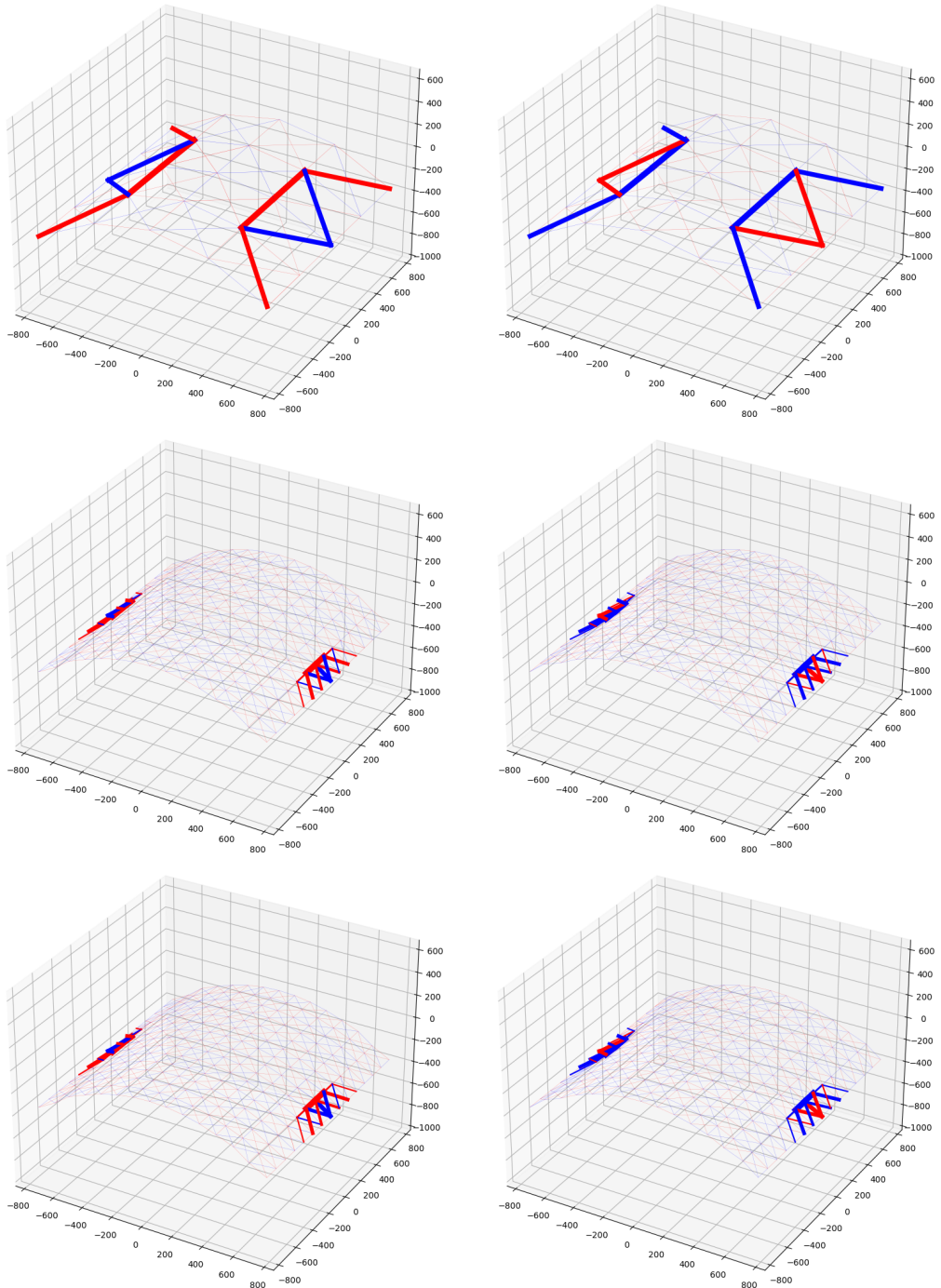


FIG. 22. Six optimal layouts of the structural shell member configuration, consistent with the six optimization results presented in Table 4. The left and right columns represent the results for kinematic loading in variants A and B, respectively.

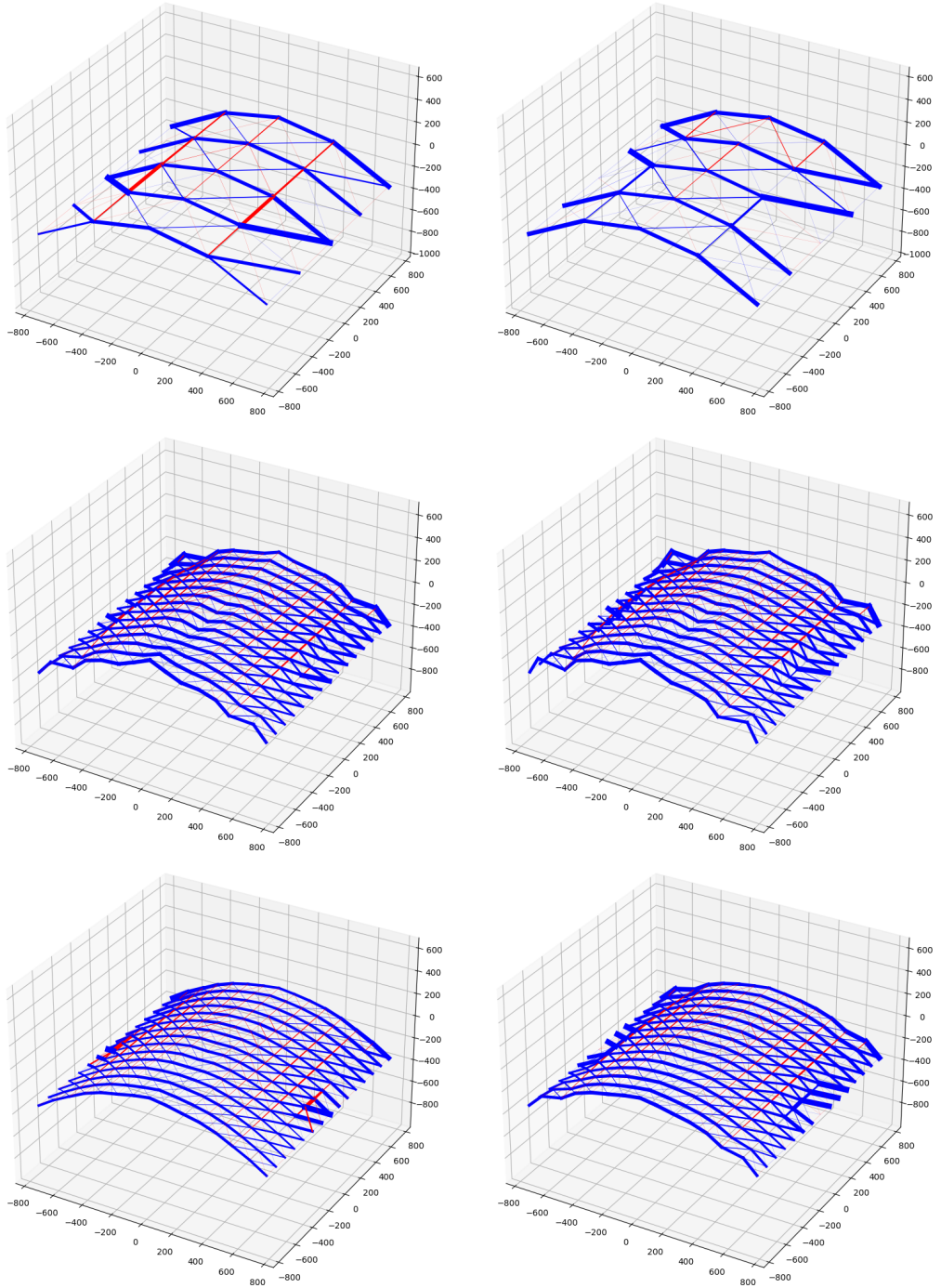


FIG. 23. Six optimal layouts of the deformed structural shell member structure consistent with the six optimization results presented in Table 5. The left and right columns represent the results for simultaneous kinematic and loading in variants A and B, respectively.

stiffness matrix singularities. Thus, post-processing in this case involves finding the displacements of the truss nodes based on the equilibrium equations (10), defined by the standard stiffness matrix, which is calculated for the optimal values of the member cross-sections. The zero optimal cross-sections are replaced with cross-sections with very small, but non-zero values.

A distinctive feature of the optimal layouts shown in Figs. 22 and 23, as well as the solutions presented in Tables 4 and 5 for the analyzed truss shell, is the increasing sensitivity of the static response of the structure to the given kinematic displacements of the supports. This sensitivity increases, with the increasing number of members (from 72 to 812 for the densities of 5×5 and 15×15 , respectively). This may suggest that, in some cases of truss structures, a static analysis based on geometrically nonlinear theory is necessary.

Let us note that when taking into account only the kinematic load, a significant increase in the maximum displacements of the nodes located inside the shell structure is observed as the density of the bar mesh increases. For example, examining the results for the trusses of variant B (Table 4, right column), we can see that the absolute value of the maximum displacement of the shell node with a sparse 5×5 mesh is 2.47 cm (see [2] Table 4), which is slightly greater than the maximum value of 2.0 cm at the support nodes; however, for the shell with a denser 15×15 mesh, the maximum absolute value of the displacement inside the structure increases by more than five times greater, reaching 10.80 cm (see [4] Table 4) for the value of the Λ parameter equal to $8.02e11 \text{ N} \cdot \text{cm}$. A four-fold increase in the Λ parameter to $4 \times 8.02e11 = 3.21e12 \text{ [N} \cdot \text{cm]}$ (which allows for a four-fold increase in the maximum volume of the optimal truss bars) had only a negligible effect on the effect of reducing the maximum displacements of the shell nodes caused by kinematic displacements. The displacement value only slightly decreased to 10.60 cm (see [6] Table 4).

When additional forces Q_y, Q_z , apart from the kinematic load, were applied to all nodes in variant B (Table 5, right column), the absolute value of the maximum displacement of a shell node with a sparse 5×5 mesh increased from 2.47 cm to 4.59 cm (see [2'] Table 5, Fig. 23₂). For the shell with a denser 15×15 mesh, the maximum absolute value of the displacement inside the structure increased to 52.48 cm, with the value of the Λ parameter equal to $8.02e11 \text{ N} \cdot \text{cm}$ (see [4'] Table 5, Fig. 23₄). However, when the maximum volume of the optimal truss members was increased fourfold (i.e., parameter $\Lambda = 4 \times 8.02e11 = 3.21e12 \text{ [N} \cdot \text{cm]}$), the maximum displacements of the shell nodes caused by both kinematic and static displacements were reduced to a much lower value of 21.64 cm, i.e., more than twice as small (see [6'] Table 5, Fig. 23₆). The effect of increasing the Λ parameter value on reducing the maximum displacements of shell nodes induced by both kinematic and static displacements is particularly

visible in Figs. 23₄, 23₆, where both the second and third rows on the right show optimal deformed shells, with a clearly visible reduction in maximum shell displacements shown in the third row. This reduction is evident when the optimal topologies are found for the four-times increase Λ parameter value compared to the value used in finding the optimal topologies of the lattice shells shown in the second row.

In summary, after conducting numerous numerical tests on various trusses loaded only statically, only kinematically, or both statically and kinematically, the thesis holds that the influence of the parameter Λ on the values of maximum displacements is clearly noticeable only when static loads are taken into account. However, the values of the maximum displacements of the shell practically do not depend on changes in the value of the parameter Λ when only kinematic loads of supports are taken into account. This finding could significantly impact design methods that ensure compliance with, for example, standard displacement conditions. The obtained results also reveal the occurrence of large displacements in the truss structure when small, permissible vertical displacements are imposed on support nodes, as demonstrated in the example of a dense mesh shell. In the case of other kinematically loaded structures, small vertical foundation settlements (e.g., in extreme cases causing rigid rotation of the entire structure) can also cause large horizontal displacements at the tops of very high stories. This behavior contrasts with the more common structural response in cases where small applied static loads cause small displacements. This characteristics may highlight the need for conducting static analysis based on equilibrium equations defined in the unknown and deformed, rather than the known and undeformed configuration, particularly in topology optimization when kinematic loads are considered.

4.6. Optimum design of the L-shaped cantilever plate

The last example presents the results of the topology optimization of a two-dimensional elastic body Ω , rather than trusses, using the IMD. This method allows for finding the optimal distributions of bulk $k^* = k^*(x)$ and shear $\mu^* = \mu^*(x)$, $x \in \Omega$ moduli, which serves as equivalents to the optimal cross-sectional areas A_k^* , $k = 1, \dots, e$, of truss rods. The goal is to minimize the work of the external load on displacements, i.e., to maximize the stiffness of the plate or truss structure while imposing constraints on the available material resources, such as the isoperimetric condition (3), (4) or (45). In both methods, applied to elastic bodies and lattice structures, the displacement fields were consistently eliminated and replaced by stress fields $\boldsymbol{\tau} = \boldsymbol{\tau}(x)$, $x \in \Omega$, or member forces N_i , $i = 1, \dots, e$, respectively. Moreover, the formulas for the minimized objective functions are derived in nearly identical ways from Castigliano's theorem.

This suggests that at least some properties of these functions, e.g., their ‘graph in R^r ’, may share similarities.

The design problem, analyzed from this perspective, was solved using a regular finite element (FE) mesh composed of 2523 quadrilateral finite elements. The L-shaped cantilever (see Fig. 24) is loaded with a vertical tangent traction $\mathbf{t} = -t \mathbf{e}_y$ of intensity $t = 0.1\sigma_0$ applied to the right lower vertical edge, where $\sigma_0 = 50$ MPa represents a plastic limit corresponding to a tensile test. The parameter $\Lambda = 649\,661$ MPa is used in the isoperimetric condition (45).

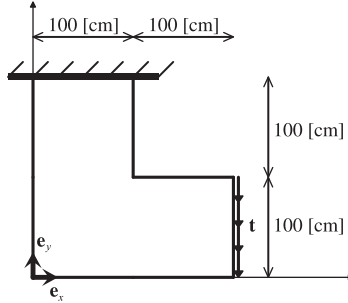


FIG. 24. The L-shaped cantilever.

The optimal layouts of the moduli k^* , μ^* , E^* have been constructed by starting the optimization process from two different initial parameter sets $\boldsymbol{\alpha} \in R^r$:

$$\text{case 1: } \boldsymbol{\alpha} = \boldsymbol{\alpha}^{\text{init}} = (0, 0, \dots, 0) \in R^r \quad (58)$$

as zero vector and

$$\text{case 2: } \boldsymbol{\alpha} = \boldsymbol{\alpha}^{\text{init}} = (\alpha_1^{\text{init}}, \alpha_2^{\text{init}}, \dots, \alpha_r^{\text{init}}) \quad (59)$$

as a vector with randomly generated components in the range $(-1000, 1000)$, i.e.,

$$\forall i = 1, 2, \dots, r, \quad \alpha_i^{\text{init}} = \text{random}(-1000, 1000). \quad (60)$$

In both cases, the parameter $\boldsymbol{\alpha}^{\text{init}} \in R^r$ initialized two different solutions:

$$\mathbf{T}^{\text{init}} = \mathbf{T}(\boldsymbol{\alpha}^{\text{init}}) = \bar{\mathbf{T}} + \sum_{k=1}^r \alpha_k^{\text{init}} \mathbf{h}_k \quad (61)$$

of the equilibrium equation:

$$\mathbf{B} \mathbf{T} = \mathbf{Q}, \quad (62)$$

where $\bar{\mathbf{T}} \in R^{3N}$ is any particular solution of (62), and

$$\mathbf{h}_k = (h_{k_1}, \dots, h_{k_{3N}}) \in R^{3N}, \quad (63)$$

($k = 1, \dots, r$) are vectors that span the kernel of the rectangular equilibrium matrix \mathbf{B} .

Similarly to the case of the truss, where the solution to the equilibrium equation (34) was defined by formula (36), the formula $\mathbf{T} = \mathbf{T}(\boldsymbol{\alpha}) = \bar{\mathbf{T}} + \sum_{k=1}^r \alpha_k \mathbf{h}_k$ (cf. (61)) also defines the solution to the equilibrium equation (62). However, the interpretation of the vectors \mathbf{T} , $\bar{\mathbf{T}}$ and spanning vectors \mathbf{h}_k of the kernel of the equilibrium matrix \mathbf{B} is of course slightly different. In this case, the components of all these vectors are not the member forces, but rather the unknown nodal stresses defining the components of the stress tensor at the nodal points. These nodal stresses are used in the polynomial interpolation of the field of statically admissible stresses in the finite elements.

In our problem $r = \dim \ker \mathbf{B} = 2700$ and $N = 2640$ represents the total number of nodes in the global finite element mesh.

The initial and optimal values of the objective function Φ for the two cases of initial starting point $\boldsymbol{\alpha}^{\text{init}}$ are:

$$\Phi^{\text{init}} = \Phi(\boldsymbol{\alpha}^{\text{init}}) = 85.45, \quad \Phi^* = \Phi(\boldsymbol{\alpha}^*) = 77.89 \text{ [MN]}, \quad (64)$$

and

$$\Phi^{\text{init}} = \Phi(\boldsymbol{\alpha}^{\text{init}}) = 1765.1, \quad \Phi^* = \Phi(\boldsymbol{\alpha}^*) = 77.97 \text{ [MN]}, \quad (65)$$

respectively. The numerically found optimal values are therefore different because the two $\boldsymbol{\alpha}^*$ minimizers in both cases are also significantly different. Both of these results translate into two, slightly different numerical values of the optimal compliance: 0.00934 and 0.00935 [MN · cm]. The optimal layouts of the elastic moduli k^* , μ^* , E^* for the two obtained solutions, shown in Fig. 25, are very similar. However, in many sub-domains of Ω , the differences in values between the optimal layouts of the same elastic moduli are substantial. The middle column in Fig. 25 shows the layouts of absolute values of the differences between the optimal values of the corresponding fields in the left and right columns.

This may suggest that either there is one global minimum, and the implemented numerical procedure cannot find the same solution from two significantly different starting points (for example, due to the global minimum being located at the bottom of a long, flat valley in the ‘objective function’s graph’) within R^{2701} Euclidean space), or there are infinitely many global minima located along one edge of this long flat valley. This scenario is similar to the presented objective function graphs in three-dimensional Euclidean space for several truss structures – see, in particular, Figs. 18–20 and Table 3 in Subsec. 4.4 for the 14-member truss.

It should be emphasized that the large differences (shown in middle column of Fig. 25) between the two solutions appear, among others, in the convex fragment

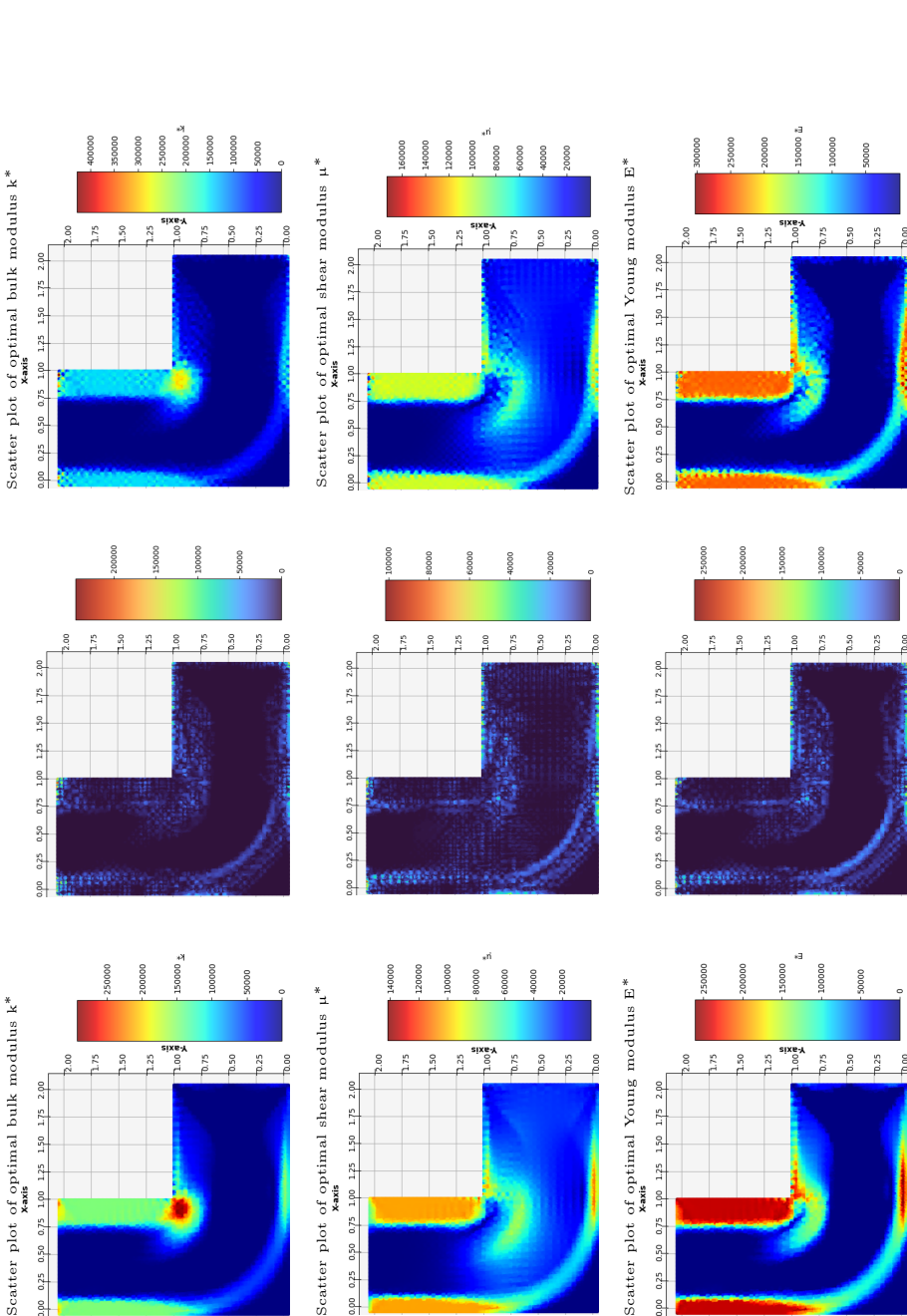


FIG. 25. In each subsequent row, the left and right columns show the optimal distribution of elastic moduli k^* , μ^* , E^* , respectively, found for two different starting points α^{init} (cases 1 and 2). The middle column displays the distributions of absolute values of the differences between the optimal moduli from the left and right sides.

shaped like a quarter-circle in the lower-left square domain of the cantilever at the reentrant corner, and along the vertical edges in the upper-left square of the cantilever, i.e. where both bulk and shear moduli (and, thus, Young's modulus) reach significant values (represented by light navy blue). On the other hand, in many other domains (mainly in the central sub-domains), where moduli k^* , μ^* , E^* reach much lower optimal values or even disappear, the differences between the two optimal solutions are close to zero (represented by dark navy blue and black).

5. Final remarks

It has been shown that when interpreting numerical results obtained from the objective function (37) in the case of truss structures discussed here (and elastic bodies – see example 4.6 and (48)), one may encounter an unexpected problem: proving the uniqueness/non-uniqueness of the optimal solution. Alternatively, there may be difficulty in demonstrating that the optimal solution was found with sufficient numerical accuracy, despite the minimized function being convex.

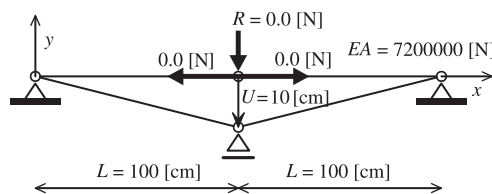
The problem indicated here is, of course, well-known and many studies have proposed various modifications to the algorithms used for searching for the minimum of a function. These modifications allow to speed up the process of numerically finding the minimum located at the bottom of almost flat (but not entirely flat) valleys. The algorithms described in [23, 24], appear particularly interesting and worth implementing – especially in the context of the IMD topology optimization, when an objective function locally resembles a long valley.

Another important consideration in practice when searching for an optimal solution, is the need to consider not one, but at least two or, as a rule, a much larger number of different load variants. A proposal for such a formulation of the problem in the context of minimizing the compliance of truss structures was already presented in [25] (see also [26] where the formulas together with algorithm for searching Pareto-optimal solutions with two independent static load variants were discussed in detail). This algorithm can be generalized to include additional kinematic load variants, as explored in this paper.

Additionally, it may be worthwhile to note at the end of the remarks concerning the stress-based version of optimization of truss structures that, based on the relationship (31), it can be stated that the absolute value of the optimal stresses, which is the same across members, not only depends explicitly on the Λ constant from the isoperimetric condition, but also depends on it implicitly. This is because each force $N_i^* = N_i^*(\Lambda)$, $i = 1, \dots, e$, also depends on this constant. Therefore, appropriately decreasing or increasing the Λ constant before restarting the optimization procedure does not guarantee an increase or

decrease in the absolute value of the stress that will appear across all members in the new optimal solution – especially in the case of trusses loaded purely by kinematic forces.

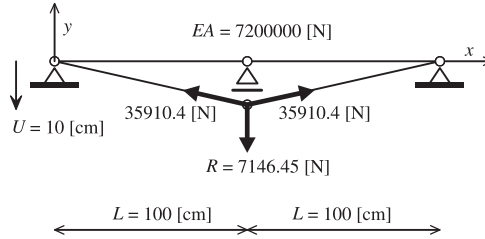
Summing up, the goal of the numerous numerical simulations presented in this paper (as well as in [14]) was to generate as many benchmarks as possible for optimal solutions to the topology optimization problem within the framework of geometrically linear truss theory. This was done before undertaking research in the field of topology optimization within the framework of geometrically nonlinear theory, taking into account static, kinematic and additionally (not mentioned in this paper) distortional loads for broadly understood truss structures. Geometric nonlinearity eliminates a number of ‘disturbing’ results of numerical solutions (see, e.g., the comment on the optimal solutions in Subsec. 4.5), as well as contradictions and paradoxes. As a trivial example, let us consider an academic problem of topology optimization problem with minimization compliance within the geometrically linear theory, in which the equilibrium equation for the once statically indeterminate, symmetrical truss composed of two horizontal members is defined in the undeformed configuration. The extreme left and right supports are fixed, while the middle support can move freely only horizontally, see Fig. 26. The displacement of the central support is forced vertically down by $|U| = 10$ cm. In Fig. 26, the ‘correct zero’ optimal solution to the topology optimization problem with minimization compliance within the geometrically linear theory is justified by the fact that, within the geometrically linear theory of trusses, such a particular support displacement, called an infinitesimal rigid (virtual) displacement when $U \rightarrow 0$ (see, e.g., [27]), does not induce a state of stress in the structure.



$$\text{Total potential energy} = -\mathbf{R} \cdot \mathbf{U} = -((-R) \times (-U)) = -(0 \times (-10)) = 0 \text{ [N} \cdot \text{cm]}$$

FIG. 26. Justification of the ‘zero’ optimal solution within the framework of geometrically linear theory for a system of two horizontal truss members.

Of course, the solution obtained by minimizing the total potential energy makes no sense from a physical point of view, because the correct solution to the statics problem, within the framework of geometrically nonlinear theory is depicted in Fig. 27, where the equilibrium equation is defined in the deformed configuration.



Total potential energy = $-\mathbf{R} \cdot \mathbf{U} = -((-R) \times (-U)) = -((-7146.45) \times (-10)) = -71464.5 \text{ [N} \cdot \text{cm]}$

FIG. 27. Correct solution to the statics problem within the framework of geometrically non-linear theory, where the equilibrium equation is defined in the deformed configuration.

References

1. A.G.M. Michell, The limits of economy of material in frames structures, *Philosophical Magazine*, **8**: 589–597, 1904, <https://doi.org/10.1080/14786440409463229>.
2. W. Hemp, *Optimum Structures*, Clarendon Press, Oxford, 1973.
3. M.P. Bendsøe, *Optimization of Structural Topology, Shape, and Material*, Springer, Berlin, 1995.
4. M.P. Bendsøe, A. Ben-Tal, J. Zowe, Optimization methods for truss geometry and topology design, *Structural Optimization*, **7**: 141–159, 1994, <https://doi.org/10.1007/BF01742459>.
5. T. Lewiński, T. Sokół, C. Graczykowski, *Michell Structures*, Springer, Cham, 2019.
6. W. Achtziger, Truss topology optimization including bar properties different for tension and compression, *Structural Optimization*, **12**: 63–74, 1996, <https://doi.org/10.1007/BF01270445>.
7. M. Gilbert, A. Tyas, Layout optimization of large-scale pin-jointed frames, *Engineering Computations*, **20**(8): 1044–1064, 2003, <https://doi.org/10.1108/02644400310503017>.
8. L. He, M. Gilbert, Rationalization of trusses generated via layout optimization, *Structural and Multidisciplinary Optimization*, **52**(4): 677–694, 2015, <https://doi.org/10.1007/s00158-015-1260-x>.
9. L. He, M. Gilbert, T. Johnson, T. Pritchard, Conceptual design of AM components using layout and geometry optimization. *Computers & Mathematics with Applications*, **78**(7): 2308–2324, 2018, <https://doi.org/10.1016/j.camwa.2018.07.012>.
10. T. Sokół, T. Lewiński, Simply supported Michell trusses generated by a lateral point load, *Structural and Multidisciplinary Optimization*, **54**: 1209–1224, 2016, <https://doi.org/10.1007/s00158-016-1480-8>.
11. K. Bołbotowski, T. Lewiński, T. Sokół, Michell structures within L-shaped domains, *Computer Assisted Mechanics and Engineering Sciences*, **27**(2–3): 185–204, 2020, <https://doi.org/10.24423/comes.281>.
12. T. Sokół, G.I.N. Rozvany, Exact truss topology optimization for external loads and friction forces, *Structural and Multidisciplinary Optimization*, **48**: 853–857, 2013, <https://doi.org/10.1007/s00158-013-0984-8>.

13. S. Czarnecki, Compliance optimization of the truss structures, *Computer Assisted Mechanics and Engineering Sciences*, **10**(2): 117–137, 2003.
14. S. Czarnecki, T. Lewiński, Trusses of the smallest total potential energy, *Bulletin of the Polish Academy of Sciences Technical Sciences*, **73**(1): e151673, 2024, <https://doi.org/10.24425/bpasts.2024.151673>.
15. C. Barbarosie, S. Lopes, A generalized notion of compliance, *Comptes Rendus Mécanique*, **339**(10): 641–648, 2011, <https://doi.org/10.1016/j.crme.2011.07.002>.
16. F. Niu, S. Xu, G. Cheng, A general formulation of structural topology optimization for maximizing structural stiffness, *Structural and Multidisciplinary Optimization*, **43**: 561–572, 2011, <https://doi.org/10.1007/s00158-010-0585-8>.
17. A. Klarbring, N. Strömberg, A note on the min-max formulation of stiffness optimization including non-zero prescribed displacements, *Structural and Multidisciplinary Optimization*, **45**: 147–149, 2012, <https://doi.org/10.1007/s00158-011-0674-3>.
18. A. Klarbring, Design optimization based on state problem functionals, *Structural and Multidisciplinary Optimization*, **52**: 417–425, 2015, <https://doi.org/10.1007/s00158-015-1240-1>.
19. S. Czarnecki, Isotropic material design, *Computational Methods in Science and Technology*, **21**(2): 49–64, 2015, <https://doi.org/10.12921/cmst.2015.21.02.001>.
20. S. Czarnecki, T. Łukasiak, Auxetic properties of the stiffest elastic bodies as a result of topology optimization and microstructures recovery based on homogenization method, *Physica Status Solidi B*, **261**(12): 2300495, 2024, <https://doi.org/10.1002/pssb.202300495>.
21. S. Czarnecki, T. Lewiński, The isotropic material design of in-plane loaded elasto-plastic plates, *Materials*, **14**(23): 7430, 2021, <https://doi.org/10.3390/ma14237430>.
22. W.H. Press, S.A. Teukolsky, W.T. Vetterling, B.P. Flannery, *Numerical Recipes in C – The Art of Scientific Computing*, 2nd ed., Cambridge University Press, Cambridge 1992.
23. A. Shterenlikht, N.A. Alexander, Levenberg–Marquardt vs Powell’s dogleg method for Gurson–Tvergaard–Needleman plasticity model, *Computer Methods in Applied Mechanics and Engineering*, **237–240**: 1–9, 2012, <https://doi.org/10.1016/j.cma.2012.04.018>.
24. Q.-X. Li, R.-Q. He, Z.-Y. Lu, Accelerating optimization by tracing valley, *Computer Physics Communications*, **203**: 168–177, 2016, <https://doi.org/10.1016/j.cpc.2016.03.002>.
25. S. Czarnecki, Edgeworth-Pareto optimal trusses of least compliance, [in:] *Mechanics and Materials*, S. Jemioło, M. Lutomirska [Eds.], pp. 61–75, Oficyna Wydawnicza Politechniki Warszawskiej, Warsaw, 2013.
26. S. Czarnecki, T. Lewiński, Optimal design of non-homogeneous isotropic material properties for the multiple loading conditions, *Physica Status Solidi B*, **254**(12): 1600821, 2017, <https://doi.org/10.1002/pssb.201600821>.
27. M.E. Gurtin, *An Introduction to Continuum Mechanics*, Academic Press, New York, 1981.

*Received November 7, 2024; revised version January 26, 2025;
accepted February 27, 2025; published online March 28, 2025.*